Simultaneous Calibration of Odometry and Sensor Parameters for Mobile Robots

Article *in* IEEE Transactions on Robotics · April 2013

DOI: 10.1109/TRO.2012.2226380

CITATIONS
76

READS
1,198

4 authors:

Andrea Censi
Massachusetts Institute of Technology
56 PUBLICATIONS **1,537** CITATIONS
SEE PROFILE

Antonio Franchi
University of Twente
170 PUBLICATIONS **3,766** CITATIONS
SEE PROFILE

Luca Marchionni
PAL Robotics
7 PUBLICATIONS **207** CITATIONS
SEE PROFILE

Giuseppe Oriolo
Sapienza University of Rome
204 PUBLICATIONS **7,313** CITATIONS
SEE PROFILE

Simultaneous Calibration of Odometry and Sensor Parameters for Mobile Robots

Andrea Censi, *Member, IEEE*, Antonio Franchi, *Member, IEEE*, Luca Marchionni, *Student Member, IEEE*, and Giuseppe Oriolo, *Senior Member, IEEE*

***Abstract*—Consider a differential-drive mobile robot equipped with an on-board exteroceptive sensor that can estimate its own motion, e.g., a range-finder. Calibration of this robot involves estimating six parameters: three for the odometry (radii and distance between the wheels) and three for the pose of the sensor with respect to the robot. After analyzing the observability of this problem, this paper describes a method for calibrating all parameters at the same time, without the need for external sensors or devices, using only the measurement of the wheel velocities and the data from the exteroceptive sensor. The method does not require the robot to move along particular trajectories. Simultaneous calibration is formulated as a maximum-likelihood problem and the solution is found in a closed form. Experimental results show that the accuracy of the proposed calibration method is very close to the attainable limit given by the Cramér–Rao bound.**

***Index Terms*—Differential-drive, extrinsic calibration, mobile robots, odometry calibration.**

I. Introduction

THE operation of a robotic system requires the *a priori* knowledge of the parameters that describe the properties and configuration of its sensors and actuators. These parameters are usually classified into *intrinsic* and *extrinsic*. By intrinsic, one usually means those parameters tied to a single sensor or actuator. Examples of intrinsic parameters include the odometry parameters or the focal length of a pinhole camera. Extrinsic parameters describe the relations among sensors/actuators such as the relative poses of their reference frames.

This paper formulates, analyzes, and solves a calibration problem comprising both the intrinsic odometry parameters of a differential-drive robot *and* the extrinsic calibration between the robot platform and an exteroceptive sensor that can estimate its egomotion. The resulting method can be used to calibrate from scratch all relevant parameters of the most common robotic configuration. No external sensors or prior information are needed. To put this contribution in perspective, we briefly review the relevant literature, starting from the most common approaches for odometry calibration.

A. Related Work for Odometry Calibration

Doebbler *et al.* [1] show that it is possible to estimate the calibration parameters using only internal odometry measurements, if the wheeled platform has enough extra measurements from caster wheels. Most commonly, one resorts to using measurements from additional sensors. For example, Von der Hardt *et al.* show that additional *internal* sensors, such as gyroscopes and compasses, can be used for odometry calibration [2]. The most popular methods consist in driving the robot along especially crafted trajectories, taking some external measurement of its pose by an *external* sensor, and then correcting a first estimate of the odometry parameters based on the knowledge of how an error in the estimated parameters affects the final pose. This approach has been pioneered by Borenstein and Feng with the *UMBmark* method [3], in which a differential-drive robot is driven repeatedly along a square path, clockwise and anticlockwise, taking an external measurement of the final pose; based on the final error, two of the three degrees of freedom can be corrected. Kelly [4] generalizes the procedure to arbitrary trajectories and different kinematics.

An alternative approach is to formulate odometry calibration as a filtering problem. A possibility is to use an extended Kalman filter (EKF) that estimates both the pose of the robot and the odometry parameters, as shown by Larsen *et al.* [5], Caltabiano *et al.* [6], and Martinelli *et al.* [7]. Foxlin [8] proposes a generalization of this idea, where the filter's state vector contains sensor parameters, robot configuration, and environment map; further research (especially by Martinelli, discussed later) has shown that one must be careful about observability issues when considering such large and heterogeneous systems, as it is not always the case that the complete state is observable.

The alternative to filtering is to solve an optimization problem, often in the form of maximum-likelihood estimation. Roy and Thrun [9] propose an online method to estimate the parameters of a simplified odometry model for a differential-drive robot. Antonelli *et al.* [10], [11] use a maximum-likelihood method to estimate the odometry parameters of a differential-drive robot, using the absolute observations of an external camera. The method is particularly simple because the problem is exactly

Manuscript received July 16, 2012; accepted October 14, 2012. Date of publication March 21, 2013; date of current version April 1, 2013. This paper was recommended for publication by Associate Editor M. Minor and Editor W. K. Chung upon evaluation of the reviewers' comments.

A. Censi is with the Control and Dynamical Systems Department, California Institute of Technology, Pasadena, CA 91125 USA (e-mail: andrea@cds.caltech.edu).

A. Franchi is with the Department of Human Perception, Cognition and Action, Max Plank Institute for Biological Cybernetics, 72076 Tübingen, Germany (e-mail: antonio.franchi@tuebingen.mpg.de).

L. Marchionni is with the Pal Robotics SL, Barcelona 08005, Spain (e-mail: luca.marchionni@pal-robotics.com).

G. Oriolo is with the Dipartimento di Ingegneria Informatica, Automatica e Gestionale, Sapienza Università di Roma, Rome I-00185, Italy (e-mail: oriolo@dis.uniroma1.it).

This paper has supplementary downloadable material available at http://ieeexplore.ieee.org.

Color versions of one or more of the figures in this paper are available online at http://ieeexplore.ieee.org.

Digital Object Identifier 10.1109/TRO.2012.2226380

linear and, therefore, can be solved with linear least squares. Antonelli and Chiaverini [12] show that the same problem can be solved with a *deterministic filter* (a nonlinear observer) obtaining largely equivalent results. Kümmerle *et al.* [13] formulate a joint estimation problem for localization, mapping, and odometry parameters. The optimization problem is solved using a numerical nonlinear optimization approach.

It is worth pointing out some general differences between the approaches. UMBmark- and EKF-like methods assume that nominal values of the parameters are known *a priori*, and only relatively small adjustments are estimated. For the EKF, the usual *caveats* apply: the linearization error might be significant, and it might be challenging to mitigate the effect of outliers in the data (originating, for example, from wheel slipping). A nonlinear observer has simpler proofs for convergence and error boundedness than an EKF, but does not provide an estimate of the uncertainty. An offline maximum-likelihood problem has the property that outliers can be dealt with easily, and it is not impacted by linearization, but an *ad hoc* solution is required for each case, because the resulting optimization problem is usually nonlinear and nonconvex.

B. Related Work for Extrinsic Sensor Calibration

In robotics, if an on-board sensor is mounted on the robot, one must estimate the sensor pose with respect to the robot frame, in addition to the odometry parameters, as a preliminary step before fusing together odometry and sensor data in problems such as localization and mapping. In related fields, problems of extrinsic calibration of exteroceptive sensors are well studied; for example, calibration of sets of cameras or stereo rigs is a typical problem in computer vision. The problem has also been studied for heterogeneous sensors, such as camera plus (3-D) range-finder [14]–[16]. Martinelli and Scaramuzza [17] consider the problem of calibrating the pose of a bearing sensor and show that the system is not fully observable as there is an unavoidable scale uncertainty. Martinelli and Siegwart [18] describe the observability properties for different combinations of sensors and kinematics. The results are not always intuitive and this motivated successive works to formally prove the observability properties of the system under investigation. Mirzaei and Roumeliotis [19] study the calibration problem for a camera and IMU using an EKF. Hesch *et al.* [20] consider the problem of estimating the pose of a camera using observations of a mirror surface with a maximum-likelihood formulation. Underwood *et al.* [21] and Brookshir and Teller [22] consider the problem of calibrating multiple exteroceptive sensors on a mobile robot. Kelly and Sukhatme [23] solve the problem of extrinsically calibrating a camera and an inertial measurement unit.

C. Calibration of Odometry and Exteroceptive Sensors

Calibrating odometry and sensor pose at the same time is a chicken-and-egg problem. In fact, the methods used to calibrate the sensor pose assume that the odometry is already calibrated, while the methods that calibrate the odometry assume that the sensor pose is known (or that an additional external sensor is present). Calibrating both at the same time is a more complicated problem that cannot be decomposed in two subproblems. In [24], we presented the first work (to the best of our knowledge) dealing with the joint calibration of intrinsic odometry parameters and extrinsic sensor pose. In particular, we considered a differential-drive robot equipped with a range-finder, or, in general, any sensor that can estimate its egomotion. This is a very common configuration used in robotics. Later, Martinelli [25] considered the simultaneous calibration of a differential-drive robot plus the pose of a *bearing sensor*, i.e., a sensor that returns the angle under which a point feature is seen. Mathematically, this is a very different problem, because, as Martinelli shows, the system is unobservable and several parameters, among which the relative pose of the bearing sensor, can be recovered only up to a scale factor. Most recently, Martinelli [26] has revisited the same problem in the context of a general treatment of estimation problems where the state cannot be fully reconstructed. The concept of *continuous symmetry* is introduced to describe such situations, in the same spirit of "symmetries" as studied in theoretical physics and mechanics (in which often "symmetry" is a synonym for the action of a Lie group), but deriving everything using the machinery of the theory of distributions as applied in nonlinear control theory. Antonelli *et al.* [27], [28] consider the problem of calibrating the odometry together with the intrinsic/extrinsic parameters of an on-board camera, assuming knowledge of a certain landmark configuration in the environment.

The method presented in [24] has several interesting characteristics: the robot drives autonomously along arbitrary trajectories, no external measurement is necessary, and no nominal parameters must be measured beforehand. Moreover, the formulation as a static maximum-likelihood problem allows us to detect and filter outliers. This paper is an extension of that work, containing a complete observability analysis proving that the system is locally observable, as well as a complete characterization of the global symmetries (see Section III); more careful treatment of some simplifying assumptions (see Section V-B1); more comprehensive experimental data, plus uncertainty and optimality analyses based on the Cramér–Rao bound (CRB) (see Section VII). The additional multimedia materials attached include a C++ implementation of the method and the log data used in the experiments.

II. Problem Formulation

Let $\mathrm{SE}(2)$ be the special Euclidean group of planar motions, and $\mathrm{se}(2)$ its Lie algebra [29]. Let $\boldsymbol{q} = (q_x, q_y, q_\theta) \in \mathrm{SE}(2)$ be the robot pose with respect to a fixed world frame (see Fig. 1). For a differential-drive robot, the pose evolves according to the differential equation

$$\dot{\boldsymbol{q}} = \begin{pmatrix} \cos q_\theta & 0 \\ \sin q_\theta & 0 \\ 0 & 1 \end{pmatrix} \begin{pmatrix} v \\ \omega \end{pmatrix}. \tag{1}$$

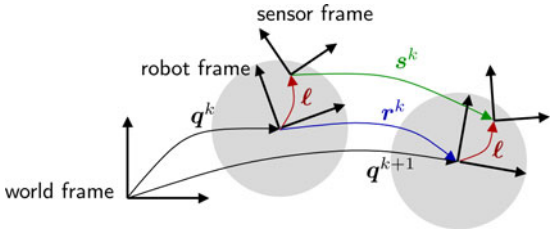

Fig. 1. Robot pose is $\boldsymbol{q}^k \in \mathrm{SE}(2)$ with respect to the world frame; the sensor pose is $\boldsymbol{\ell} \in \mathrm{SE}(2)$ with respect to the robot frame; $\boldsymbol{r}^k \in \mathrm{SE}(2)$ is the robot displacement between poses; and $\boldsymbol{s}^k \in \mathrm{SE}(2)$ is the displacement seen by the sensor in its own reference frame.

The driving velocity v and the steering velocity ω depend on the left and right wheel velocities $\omega_{\mathrm{L}}, \omega_{\mathrm{R}}$ by a linear transformation

$$\begin{pmatrix} v \\ \omega \end{pmatrix} = \boldsymbol{J} \begin{pmatrix} \omega_{\mathrm{L}} \\ \omega_{\mathrm{R}} \end{pmatrix}. \tag{2}$$

The matrix $\boldsymbol{J}$ is a function of the parameters r_{L}, r_{R}, and b

$$\boldsymbol{J} = \begin{pmatrix} J_{11} & J_{12} \\ J_{21} & J_{22} \end{pmatrix} = \begin{pmatrix} +r_{\mathrm{L}}/2 & +r_{\mathrm{R}}/2 \\ -r_{\mathrm{L}}/b & +r_{\mathrm{R}}/b \end{pmatrix} \tag{3}$$

where r_{L} and r_{R} are the left and right wheel radii, respectively, and b is the distance between the wheels. We assume that we can measure the wheel velocities ω_{L} and ω_{R}. We do not assume to be able to *set* the wheel velocities; this method is entirely passive and works with any trajectory, if it satisfies the necessary excitability conditions, which are outlined in the next section.

We also assume that there is an exteroceptive sensor mounted horizontally (with zero pitch and roll) on the robot. Therefore, the pose of the sensor can be represented as $\boldsymbol{\ell} = (\ell_x, \ell_y, \ell_\theta) \in \mathrm{SE}(2)$ with respect to the robot frame (see Fig. 1). Thus, at any given time t, the pose of the sensor in the world frame is $\boldsymbol{q}(t) \oplus \boldsymbol{\ell}$, where "$\oplus$" is the group operation on $\mathrm{SE}(2)$. The definitions of "$\oplus$" and the group inverse "$\ominus$" are recalled in Table I.

The exteroceptive observations are naturally a discrete process $\boldsymbol{m}^k$: observations are available at a set of time instants $t_1 < \cdots < t_k < \cdots < t_n$, which are not necessarily equispaced in time. Consider the generic kth interval $t \in [t_k, t_{k+1}]$. Let the initial and final poses of the robot be $\boldsymbol{q}^k = \boldsymbol{q}(t_k)$ and $\boldsymbol{q}^{k+1} = \boldsymbol{q}(t_{k+1})$, respectively. Denote by $\boldsymbol{s}^k$ the displacement of the sensor during the interval $[t_k, t_{k+1}]$; this corresponds to the motion between $\boldsymbol{q}^k \oplus \boldsymbol{\ell}$ and $\boldsymbol{q}^{k+1} \oplus \boldsymbol{\ell}$ (see Fig. 1) and can be written as

$$\boldsymbol{s}^k = \ominus \left(\boldsymbol{q}^k \oplus \boldsymbol{\ell}\right) \oplus \left(\boldsymbol{q}^{k+1} \oplus \boldsymbol{\ell}\right).$$

Letting $\boldsymbol{r}^k = \ominus \boldsymbol{q}^k \oplus \boldsymbol{q}^{k+1}$ be the robot displacement in the interval, the sensor displacement can also be written as

$$\boldsymbol{s}^k = \ominus \boldsymbol{\ell} \oplus \boldsymbol{r}^k \oplus \boldsymbol{\ell}. \tag{4}$$

We assume that it is possible to estimate the sensor's egomotion $\boldsymbol{s}^k$ given the exteroceptive measurements $\boldsymbol{m}^k$ and $\boldsymbol{m}^{k+1}$, and we call $\hat{\boldsymbol{s}}^k$ such estimate (for example, if the sensor is a range-finder, the egomotion can be estimated via scan matching). At this point, the problem can be stated formally.

TABLE I
SYMBOLS USED IN THIS PAPER

Calibration parameters to be estimated	
$r_{\mathrm{R}}, r_{\mathrm{L}}$	wheel radii
b	distance between wheels
$\boldsymbol{\ell}$	sensor pose relative to robot frame
Robot kinematics	
$\boldsymbol{q}$	robot pose relative to world frame
ω_{L}, ω_{R}	left/right wheel velocity
v, ω	driving/steering robot velocities
$\boldsymbol{J}$	linear map between wheel and robot velocities
Sensing process	
$\boldsymbol{m}^k$	exteroceptive measurements, available at time t_k
$\boldsymbol{r}^k$	robot displacement in the k-th interval $[t_k, t_{k+1}]$
$\boldsymbol{s}^k$	sensor displacement in the k-th interval
$\hat{\boldsymbol{s}}^k$	sensor displacement estimated from $\boldsymbol{m}^k$ and $\boldsymbol{m}^{k+1}$
$\boldsymbol{\nu}$	sensor velocity in the sensor frame
Other symbols	
$\oplus$, $\ominus$	"$\oplus$" is the group operation on $\mathrm{SE}(2)$: $\begin{pmatrix} a_x \\ a_y \\ a_\theta \end{pmatrix} \oplus \begin{pmatrix} b_x \\ b_y \\ b_\theta \end{pmatrix} = \begin{pmatrix} a_x + b_x \cos(a_\theta) - b_y \sin(a_\theta) \\ a_y + b_x \sin(a_\theta) + b_y \cos(a_\theta) \\ a_\theta + b_\theta \end{pmatrix}$ "$\ominus$" is the group inverse: $\ominus \begin{pmatrix} a_x \\ a_y \\ a_\theta \end{pmatrix} = \begin{pmatrix} -a_x \cos(a_\theta) - a_y \sin(a_\theta) \\ +a_x \sin(a_\theta) - a_y \cos(a_\theta) \\ -a_\theta \end{pmatrix}$

Problem 1 (Simultaneous calibration): Given the wheel velocities $\omega_{\mathrm{L}}(t)$ and $\omega_{\mathrm{R}}(t)$ for $t \in [t_1, t_n]$, and the estimated sensor egomotion $\hat{\boldsymbol{s}}^k$ $(k = 1, \ldots, n-1)$ corresponding to the exteroceptive observations at times $t_1 < \cdots < t_k < \cdots < t_n$, find the maximum-likelihood estimate for the parameters $r_{\mathrm{L}}, r_{\mathrm{R}}, b, \ell_x, \ell_y,$ and ℓ_θ.

III. OBSERVABILITY ANALYSIS

It has become (good) praxis in robotics to provide an observability analysis prior to solving an estimation problem. In robotics, we have systems that evolve according to a continuous-time dynamics, but observations from the sensors are typically discrete. There are at least three ways to prove observability, which consider different aspects of the model.

1) One kind of observability is equivalent to proving that the system is locally weakly observable, in the control-theory sense [30]. To apply this analysis, it is required that the system is in the continuous-time form

$$\begin{aligned} \dot{\boldsymbol{x}} &= \boldsymbol{f}(\boldsymbol{x}, \boldsymbol{u}) \\ \boldsymbol{y} &= \boldsymbol{g}(\boldsymbol{x}) \end{aligned} \tag{5}$$

where $\boldsymbol{x}$ contains both parameters and time-varying state, and $\boldsymbol{y}$ are continuous-time observations. The proof usually consists in computing successive Lie derivatives and is a proof of existence of some exciting commands, but it is not usually constructive. These techniques are intrinsically nonlinear. Such analysis does not take into account the uncertainty in the observations.

2) The alternative is a "static" analysis, which supposes that the system is in the form $\boldsymbol{y} = \boldsymbol{h}(\boldsymbol{x}, \boldsymbol{u})$, where $\boldsymbol{y}$ is now a vector of discretized observations. The analysis consists in showing constructively that, for certain values of the commands $\boldsymbol{u}$, there are enough constraints as to uniquely determine $\boldsymbol{x}$.

3) A stochastic analysis based on the Fisher Information Matrix (FIM) [31] assumes that the system is in the static form

$$\boldsymbol{y} = \boldsymbol{h}(\boldsymbol{x}, \boldsymbol{u}) + \boldsymbol{\epsilon} \tag{6}$$

and $\boldsymbol{\epsilon}$ is additive stochastic noise. The system is said to be observable if the FIM of $\boldsymbol{x}$ is full rank, when $\boldsymbol{u}$ is chosen appropriately.

These formalizations have different properties; continuous-time and discrete-time modeling of the same system could reveal different aspects; in addition, the FIM analysis corresponds to a linearized analysis, but it also allows a quantitative bound on the uncertainty. A discrete-time formalization is better suited for our system, as the problem is naturally discretized by the exteroceptive sensor observations. The following statements show that the system is observable in the "static" sense. The uncertainty estimation for the method is done using the FIM. This allows us to check not only that the system is observable, but also how well conditioned the constraints are.

1) Global Ambiguities: There is a global ambiguity of the parametrization.

Proposition 2: The two sets of calibration parameters $(r_{\mathrm{L}}, r_{\mathrm{R}}, b, \ell_x, \ell_y, \ell_\theta)$ and $(-r_{\mathrm{L}}, -r_{\mathrm{R}}, -b, -\ell_x, -\ell_y, \ell_\theta + \pi)$ are indistinguishable.

(See Appendix A for a proof.) By convention, we will choose the solution with $b > 0$ so that b has the physical interpretation of the (positive) distance between the wheels. We also assume throughout the paper that $r_{\mathrm{L}}, r_{\mathrm{R}} \neq 0$. Negative radii are allowed, accounting for the fact that the wheel might be mounted in the opposite direction (i.e., it spins clockwise, rather than counterclockwise). We will give a constructive proof that this is the only ambiguity, as we will show that the maximum-likelihood problem has a unique solution once the ambiguity of Proposition 2 is resolved.

2) Observability: We will prove that the parameters are observable from the observations of just two intervals (there are six parameters and each interval gives three observations), provided that the trajectories are "independent," as defined below. Let the total left wheel rotation in the kth interval be $\Delta_L^k = \int_{t_k}^{t_{k+1}} \omega_{\mathrm{L}}(t)dt$, and analogously define Δ_R^k. Moreover, let $\mathrm{Log} : \mathrm{SE}(2) \to \mathrm{se}(2)$ be the logarithmic map on $\mathrm{SE}(2)$.

Proposition 3: All calibration parameters are observable if and only if the dataset contains at least one pair of trajectories that satisfy the following conditions.

1) The vectors $(\Delta_L^1 \ \Delta_R^1)^T$ and $(\Delta_L^2 \ \Delta_R^2)^T$ are linearly independent.
2) The motions $\boldsymbol{r}^1$ and $\boldsymbol{r}^2$ are "independent," in the sense that there exists no $\gamma \in \mathbb{R}$ such that

$$\log(\boldsymbol{r}^1) = \gamma \log(\boldsymbol{r}^2). \tag{7}$$

3) The motions $\boldsymbol{r}^1$ and $\boldsymbol{r}^2$ are not both pure translations.

(See Appendix B for a proof.) Note that the second property is a *generic* property, in the sense that, fixed $\boldsymbol{r}^1$, almost all displacements $\boldsymbol{r}^2$ make the parameters observable. Note also that both conditions refer to the total displacement (of wheels and robot, respectively), but it does not matter for observability the exact trajectory followed by the robot. For the particular case of trajectories with constant velocities, the conditions can be further simplified.

Corollary 4: In the case of trajectories of constant velocity, the parameters are observable if and only if *the vectors containing the constant wheel velocities* $(\omega_L^1 \ \omega_R^1)^T$ and $(\omega_L^2 \ \omega_R^2)^T$ are linearly independent (for example, a pure rotation and a pure forward translation).

IV. Maximum-Likelihood Formalization of the Calibration Problem

Formulating the problem as a maximum-likelihood problem means seeking the parameters that best explain the measurements and involves deriving the objective function (the measurement log-likelihood) as a function of the parameters and the measurements. Consider the robot motion along an arbitrary configuration trajectory $\boldsymbol{q}(t)$ with observations at times $t_1 < \cdots < t_k < \cdots < t_n$. Consider the kth interval, in which the robot moves from pose $\boldsymbol{q}^k = \boldsymbol{q}(t_k)$ to pose $\boldsymbol{q}^{k+1} = \boldsymbol{q}(t_{k+1})$. The robot pose displacement is $\boldsymbol{r}^k = \ominus \boldsymbol{q}^k \oplus \boldsymbol{q}^{k+1}$. This quantity depends on the wheel velocities $\omega_{\mathrm{L}}(t)$, $\omega_{\mathrm{R}}(t)$, for $t \in [t_k, t_{k+1}]$, as well as the odometry parameters. To highlight this dependence, we write $\boldsymbol{r}^k = \boldsymbol{r}^k(r_{\mathrm{L}}, r_{\mathrm{R}}, b)$. We also rewrite (4), which gives the constraint between $\boldsymbol{r}^k$, the sensor displacement $\boldsymbol{s}^k$, and the sensor pose $\boldsymbol{\ell}$, evidencing the dependence on the odometry parameters

$$\boldsymbol{s}^k = \ominus \boldsymbol{\ell} \oplus \boldsymbol{r}^k(r_{\mathrm{L}}, r_{\mathrm{R}}, b) \oplus \boldsymbol{\ell}. \tag{8}$$

We assume to know an estimate $\hat{\boldsymbol{s}}^k$ of the sensor displacement, distributed as a Gaussian[1] with mean $\boldsymbol{s}^k$ and known covariance $\boldsymbol{\Sigma}_k$. The log-likelihood $\mathcal{J} = \log p(\{\hat{\boldsymbol{s}}^k\} | r_{\mathrm{L}}, r_{\mathrm{R}}, b, \boldsymbol{\ell})$ is

$$\mathcal{J} = -\frac{1}{2} \sum_{k=1}^{n} \| \hat{\boldsymbol{s}}^k - \ominus \boldsymbol{\ell} \oplus \boldsymbol{r}^k(r_{\mathrm{L}}, r_{\mathrm{R}}, b) \oplus \boldsymbol{\ell} \|^2_{\boldsymbol{\Sigma}_k^{-1}} \tag{9}$$

where $\|\boldsymbol{z}\|^2_{\boldsymbol{A}} = \boldsymbol{z}^T \boldsymbol{A} \boldsymbol{z}$ is the $\boldsymbol{A}$-norm of a vector $\boldsymbol{z}$. We have reduced calibration to an optimization problem.

Problem 5 (Simultaneous calibration, maximum-likelihood formulation): Maximize (9) with respect to $r_{\mathrm{L}}, r_{\mathrm{R}}, b, \ell_x, \ell_y, \ell_\theta$.

This maximization problem is nonconvex; therefore, it cannot be solved efficiently by general-purpose numerical techniques [32]. However, we can still solve it in a closed form, according to the algorithm described in the next section.

V. Calibration Method

This section describes an algorithmic solution to Problem 5. The method is summarized in Algorithm 1. The algorithm provides the exact solution to the problem, if the following technical assumption holds.

Assumption 1: The covariance $\boldsymbol{\Sigma}_k$ of the estimate $\hat{\boldsymbol{s}}^k$ is diagonal and isotropic in the x- and y-directions

$$\boldsymbol{\Sigma}_k = \mathrm{diag}((\sigma_{xy}^k)^2, (\sigma_{xy}^k)^2, (\sigma_\theta^k)^2).$$

[1]We treat $\mathrm{SE}(2)$ as a vector space under the assumption that the error of $\hat{\boldsymbol{s}}^k$ is small. More precisely, the vector-space approximation is implicit in stating that the distribution of $\hat{\boldsymbol{s}}^k$ is Gaussian, and, later, in (9), when writing the norm of the difference $\|\boldsymbol{a} - \boldsymbol{b}\|_{\boldsymbol{A}}$ for $\boldsymbol{a}, \boldsymbol{b} \in \mathrm{SE}(2)$.

Algorithm 1 Simultaneous calibration of odometry and sensor parameters

1) Passively collect measurements over any sufficiently exciting trajectory.
2) For each interval, run the sensor displacement algorithm to obtain the estimates $\hat{\boldsymbol{s}}^k$.
   Each interval thus contributes the data sample
   $$\langle \hat{\boldsymbol{s}}^k, \omega_{\mathrm{L}}(t), \omega_{\mathrm{R}}(t) \rangle, \qquad t \in [t_k, t_{k+1}].$$
3) Repeat N times (for outlier rejection):
   Linear estimation of J_{21}, J_{22}:
   a) For all samples, compute the matrix $\boldsymbol{L}_k$ using (10).
   b) Form the matrix $\sum_k \boldsymbol{L}_k^T \boldsymbol{L}_k$. If the condition number of this matrix is over a threshold, declare the problem underconstrained and stop.
   c) Compute J_{21}, J_{22} using (11).
   Nonlinear estimation of the calibration parameters:
   d) For all samples, compute c_x^k, c_y^k (19–20) and $\boldsymbol{Q}_k$ using (22).
   e) Let $\boldsymbol{M} = \sum_k \boldsymbol{Q}_k^T \boldsymbol{Q}_k$.
   f) Compute the coefficients a, b, c using to (28–30) and find the two candidates $\lambda^{(1)}, \lambda^{(2)}$.
   g) For each $\lambda^{(i)}$:
      i) Compute the 5×5 matrix $\boldsymbol{N}^{(i)} = \boldsymbol{M} - \lambda^{(i)} \boldsymbol{W}$.
      ii) If the rank of $\boldsymbol{N}^{(i)}$ is less than 4, declare the problem underconstrained and stop.
      iii) Find a vector $\boldsymbol{\gamma}^{(i)}$ in the kernel of $\boldsymbol{N}^i$.
      iv) Compute $\boldsymbol{\varphi}^{(i)}$ using (31).
   h) Choose the optimal $\boldsymbol{\varphi}$ between $\boldsymbol{\varphi}^{(1)}$ and $\boldsymbol{\varphi}^{(2)}$ by computing the objective function.
   i) Compute the other parameters using (32).
   Outlier rejection:
   j) Compute the χ-value of each sample using (33).
   k) Discard a fraction α of samples with the highest χ.

The covariance $\boldsymbol{\Sigma}_k$ ultimately depends on the environment features (e.g., it will be more elongated in the x-direction if there are less features that allow us to localize in that direction); as such, it is partly under the control of the user.

If the assumption does not hold, then it is recommended to use the technique of *covariance inflation*; this consists in neglecting the off-diagonal correlations, and inflating the diagonal elements. This guarantees that the estimate found is still consistent (i.e., the estimated covariance is a conservative approximation of the actual covariance).

Algorithm overview: Our plan for solving the problem consists of the following steps, which will be detailed in the rest of the section.

1) Linear estimation of J_{21}, J_{22} We show that it is possible to solve for the parameters $J_{21} = -r_{\mathrm{L}}/b$, $J_{22} = r_{\mathrm{R}}/b$ independently of the others by considering only the rotation measurements $\hat{s}_\theta^k$. In fact, s_θ^k depends linearly on J_{21}, J_{22}; therefore, the parameters can be recovered easily and robustly via linear least squares. This first part of the algorithm is equivalent to the procedure in [10] and [11].

2) Nonlinear estimation of the other parameters

a) *Treatable approximation of the likelihood.*
We show that, under Assumption 1, it is possible to write the term $\|\hat{\boldsymbol{s}}^k - \ominus \boldsymbol{\ell} \oplus \boldsymbol{r}^k \oplus \boldsymbol{\ell}\|$ in (9) as $\|\boldsymbol{\ell} \oplus \hat{\boldsymbol{s}}^k - \boldsymbol{r}^k \oplus \boldsymbol{\ell}\|$, which is easier to minimize.

b) *Integration of the kinematics.*
We show that, given the knowledge of J_{21}, J_{22}, for any trajectory, the translation (r_x^k, r_y^k) is a linear function of the wheel axis length b.

c) *Constrained quadratic optimization formulation.*
We use the trick of considering $\cos \ell_\theta, \sin \ell_\theta$ as two separate variables. This allows us to write the original objective function as a quadratic function of the vector $\boldsymbol{\varphi} = (\, b \quad \ell_x \quad \ell_y \quad \cos \ell_\theta \quad \sin \ell_\theta \,)^T$, which contains all four remaining parameters. The constraint $\varphi_4^2 + \varphi_5^2 = 1$ is added to ensure consistency.

d) *Solution of the constrained quadratic system.*
We show that the constrained quadratic problem can be solved in closed form; thus, we can estimate the parameters $b, \ell_x, \ell_y, \ell_\theta$.

e) *Recovering $r_{\mathrm{L}}, r_{\mathrm{R}}$.*
The radii are estimated from J_{21}, J_{22}, and b.

3) Outlier removal. An outlier detection/rejection phase must be integrated in the algorithm to deal with slipping and other sources of unmodeled errors.

4) Uncertainty estimation. The uncertainty of the solution is computed using the CRB.

A. Linear Estimation of J_{21}, J_{22}

The two parameters $J_{21} = -r_{\mathrm{L}}/b$ and $J_{22} = r_{\mathrm{R}}/b$ can be estimated by solving a weighted least squares problem. This subproblem is entirely equivalent to the procedure described in [10] and [11].

First, note that the constraint equation (8) implies that $s_\theta^k = r_\theta^k$: the robot and the sensor see the same rotation.

From the kinematics of the robot, we know that the rotational displacement of the robot is a linear function of the wheel velocities and the odometry parameters. More precisely, from (1) and (2), we have $r_\theta^k = \boldsymbol{L}_k \begin{pmatrix} J_{21} \\ J_{22} \end{pmatrix}$, with $\boldsymbol{L}_k$ a row vector that depends on the velocities

$$\boldsymbol{L}_k = \left(\int_{t_k}^{t_{k+1}} \omega_{\mathrm{L}}(t) dt \quad \int_{t_k}^{t_{k+1}} \omega_{\mathrm{R}}(t)\, dt \right). \tag{10}$$

Using the available estimate $\hat{s}_\theta^k$ of s_θ^k, with standard deviation σ_θ^k, an estimate of J_{21}, J_{22} can be found via linear least squares as

$$\begin{pmatrix} \hat{J}_{21} \\ \hat{J}_{22} \end{pmatrix} = \left[\sum_k \frac{\boldsymbol{L}_k^T \boldsymbol{L}_k}{\left(\sigma_\theta^k\right)^2} \right]^{-1} \sum_k \frac{\boldsymbol{L}_k^T}{\left(\sigma_\theta^k\right)^2} \hat{s}_\theta^k. \tag{11}$$

The matrix $\sum_k \boldsymbol{L}_k^T \boldsymbol{L}_k$ is invertible if the trajectories are exciting; otherwise, the problem is underconstrained.

B. Nonlinear Estimation of the Other Parameters

We now assume that the parameters $J_{21} = -r_{\mathrm{L}}/b$ and $J_{22} = r_{\mathrm{R}}/b$ have already been estimated. The next step solves for the parameters $b, \ell_x, \ell_y, \ell_\theta$. When b is known, one can then recover $r_{\mathrm{R}}, r_{\mathrm{L}}$ from J_{21} and J_{22}.

1) Treatable Likelihood Approximation: The first step is to simplify expression (9) for the log-likelihood. For the standard 2-norm, the following equivalence holds:

$$\|\boldsymbol{s}^k - \ominus\boldsymbol{\ell} \oplus \boldsymbol{r}^k \oplus \boldsymbol{\ell}\|_2 = \|\boldsymbol{\ell} \oplus \boldsymbol{s}^k - \boldsymbol{r}^k \oplus \boldsymbol{\ell}\|_2.$$

Intuitively, the two vectors on the left- and right-hand side represent the same quantity in two different reference frames; therefore, they have the same norm. This is not true for a generic matrix norm. However, it is true for the $\boldsymbol{\Sigma}_k^{-1}$-norm, which, thanks to Assumption 1 above, is isotropic in the x- and y-directions and hence rotation-invariant. Therefore, the log-likelihood (9) can be written as

$$\mathcal{J} = -\frac{1}{2}\sum_k \|\boldsymbol{\ell} \oplus \hat{\boldsymbol{s}}^k - \boldsymbol{r}^k \oplus \boldsymbol{\ell}\|^2_{\boldsymbol{\Sigma}_k^{-1}}. \tag{12}$$

2) Integrating the Kinematics: Let $\boldsymbol{r}(t) = \ominus\boldsymbol{q}^k \oplus \boldsymbol{q}(t)$, $t \geq t_k$, be the incremental robot displacement since the time t_k of the last exteroceptive observation. We need an explicit expression for $\boldsymbol{r}^k$ as a function of the parameters. We show that, if J_{21}, J_{22} are known, the displacement can be written as a linear function of the parameter b.

The displacement $\boldsymbol{r}(t)$ is the robot pose in a reference frame where the initial $\boldsymbol{q}^k$ is taken as the origin. It satisfies this differential equation with a boundary condition

$$\dot{\boldsymbol{r}} = \begin{pmatrix} \dot{r}_x \\ \dot{r}_y \\ \dot{r}_\theta \end{pmatrix} = \begin{pmatrix} v\ \cos r_\theta \\ v\ \sin r_\theta \\ \omega \end{pmatrix}, \quad \boldsymbol{r}(t_k) = \boldsymbol{0}. \tag{13}$$

The solution of this differential equation can be written explicitly as a function of the robot velocities. The solution for the rotation component r_θ is simply the integral of the angular velocity ω: $r_\theta(t) = \int_{t_k}^{t} \omega(\tau)d\tau$. Because $\omega = J_{21}\omega_{\mathrm{L}} + J_{22}\omega_{\mathrm{R}}$, the rotation component depends only on known quantities; therefore, it can be estimated as

$$r_\theta(t) = \int_{t_k}^{t} \left(J_{21}\omega_{\mathrm{L}}(\tau) + J_{22}\omega_{\mathrm{R}}(\tau)\right) d\tau. \tag{14}$$

After $r_\theta(t)$ has been computed, the solution for the translation components r_x, r_y can be written as

$$r_x(t) = \int_{t_k}^{t} v(\tau)\ \cos\ r_\theta(\tau)d\tau \tag{15}$$

$$r_y(t) = \int_{t_k}^{t} v(\tau) \sin\ r_\theta(\tau)d\tau. \tag{16}$$

Using the fact that

$$v = J_{11}\omega_{\mathrm{L}} + J_{12}\omega_{\mathrm{R}} = b\left(-\frac{1}{2}J_{21}\omega_{\mathrm{L}} + \frac{1}{2}J_{22}\omega_{\mathrm{R}}\right) \tag{17}$$

the final values $r_x^k = r_x(t_{k+1})$, $r_y^k = r_y(t_{k+1})$ can be written as a linear function of the unknown parameter b

$$r_x^k = c_x^k\, b, \quad r_y^k = c_y^k\, b \tag{18}$$

where the two constants c_x^k, c_y^k are a function of known data

$$c_x^k = \frac{1}{2}\int_{t_k}^{t_{k+1}} \left(-J_{21}\omega_{\mathrm{L}}(\tau) + J_{22}\omega_{\mathrm{R}}(\tau)\right)\cos r_\theta^k(\tau)d\tau \tag{19}$$

$$c_y^k = \frac{1}{2}\int_{t_k}^{t_{k+1}} \left(-J_{21}\omega_{\mathrm{L}}(\tau) + J_{22}\omega_{\mathrm{R}}(\tau)\right)\sin r_\theta^k(\tau)d\tau. \tag{20}$$

For a generic trajectory, three integrals are needed to find c_x^k, c_y^k, given by (14) and (18). If the wheel velocities are constant in the interval $[t_k, t_{k+1}]$, then a simplified closed form can be used, shown later in Section V-E.

3) Formulation as a Quadratic System: We now use the trick of treating $\cos\ell_\theta$ and $\sin\ell_\theta$ as two independent variables. If we group the remaining parameters in the vector $\boldsymbol{\varphi} \in \mathbb{R}^5$ as

$$\boldsymbol{\varphi} = \begin{pmatrix} b & \ell_x & \ell_y & \cos\ell_\theta & \sin\ell_\theta \end{pmatrix}^T \tag{21}$$

then (12) can be written as a quadratic function of $\boldsymbol{\varphi}$. More in detail, defining the 2×5 matrix $\boldsymbol{Q}_k$ of known coefficients as

$$\boldsymbol{Q}_k = \frac{1}{\sigma_{xy}^k}\begin{pmatrix} -c_x^k & 1-\cos\hat{r}_\theta^k & +\sin\hat{r}_\theta^k & +\hat{s}_x^k & -\hat{s}_y^k \\ -c_y^k & -\sin\hat{r}_\theta^k & 1-\cos\hat{r}_\theta^k & +\hat{s}_y^k & +\hat{s}_x^k \end{pmatrix} \tag{22}$$

the log-likelihood function (12) can be written compactly as $-\frac{1}{2}\boldsymbol{\varphi}^T\boldsymbol{M}\boldsymbol{\varphi} + \text{constant}$ with $\boldsymbol{M} = \sum_k \boldsymbol{Q}_k^T\boldsymbol{Q}_k$. We have reduced the maximization of the likelihood to a quadratic problem with a quadratic constraint

$$\min \quad \boldsymbol{\varphi}^T\boldsymbol{M}\boldsymbol{\varphi} \tag{23}$$

$$\text{subject to} \quad \varphi_4^2 + \varphi_5^2 = 1. \tag{24}$$

Constraint (24), corresponding to $\cos^2\ell_\theta + \sin^2\ell_\theta = 1$, is necessary to enforce geometric consistency.

Note that so far the solution is not fully constrained. If the vector $\boldsymbol{\varphi}^\star$ is a solution of the problem, then $-\boldsymbol{\varphi}^\star$ is equally feasible and optimal. This phenomenon corresponds to the symmetry described by Proposition 2. To make the problem fully constrained, we add another constraint for $\boldsymbol{\varphi}$ that corresponds to choosing a positive axis b

$$\varphi_1 \geq 0. \tag{25}$$

4) Solving the Constrained Least-Squares Problem: Because the objective function is bounded below, and the feasible set is closed, at least an optimal solution exists. We obtain optimality conditions using the method of Lagrange multipliers. The constraint (24) is written in matrix form as

$$\boldsymbol{\varphi}^T\boldsymbol{W}\boldsymbol{\varphi} = 1, \quad \text{with } \boldsymbol{W} = \begin{pmatrix} \boldsymbol{0}_{3\times3} & \boldsymbol{0}_{3\times2} \\ \boldsymbol{0}_{2\times3} & \boldsymbol{I}_{2\times2} \end{pmatrix}. \tag{26}$$

Consider the Lagrangian $\mathcal{L} = \boldsymbol{\varphi}^T\boldsymbol{M}\boldsymbol{\varphi} + \lambda(\boldsymbol{\varphi}^T\boldsymbol{W}\boldsymbol{\varphi} - 1)$. In this problem, Slater's condition holds; thus the Karush–Kuhn–Tucker conditions are necessary for optimality

$$\frac{\partial\mathcal{L}}{\partial\boldsymbol{x}}^T = 2\left(\boldsymbol{M} + \lambda\boldsymbol{W}\right)\boldsymbol{\varphi} = \boldsymbol{0}. \tag{27}$$

Equation (27) implies that one needs to find λ such that the matrix $(\boldsymbol{M} + \lambda\boldsymbol{W})$ is singular, and then to find the solution $\boldsymbol{\varphi}$ in the kernel of such matrix. The value of λ can be found by solving the equation $\det(\boldsymbol{M} + \lambda\boldsymbol{W}) = 0$.

For an arbitrary $\boldsymbol{M}$, the expression $\det(\boldsymbol{M} + \lambda\boldsymbol{W})$ is a fifth-order polynomial in λ. However, the polynomial is only of the second order for the matrix $\boldsymbol{M} = \sum_k \boldsymbol{Q}_k^T\boldsymbol{Q}_k$, due to repeated entries in $\boldsymbol{Q}_k$. One can show that $\boldsymbol{M}$ has the following structure

(note the zeros and repeated entries)

$$\boldsymbol{M} = \begin{pmatrix} m_{11} & 0 & m_{13} & m_{14} & m_{15} \\ & m_{22} & 0 & m_{35} & -m_{34} \\ & & m_{22} & m_{34} & m_{35} \\ & & & m_{44} & 0 \\ \text{(symmetric)} & & & & m_{44} \end{pmatrix}.$$

The determinant of $(\boldsymbol{M} + \lambda \boldsymbol{W})$ is a second-order polynomial $a_2\,\lambda^2 + a_1\,\lambda + a_0$, where the values of the coefficients can be computed as follows:

$$a_2 = m_{11}{m_{22}}^2 - m_{22}{m_{13}}^2 \tag{28}$$

$$\begin{aligned} a_1 = {} & 2m_{13}m_{22}m_{35}m_{15} - {m_{22}}^2{m_{15}}^2 \\ & + 2m_{13}m_{22}m_{34}m_{14} - 2m_{22}{m_{13}}^2m_{44} - {m_{22}}^2{m_{14}}^2 \\ & + 2m_{11}{m_{22}}^2m_{44} + {m_{13}}^2{m_{35}}^2 - 2m_{11}m_{22}{m_{34}}^2 \\ & + {m_{13}}^2{m_{34}}^2 - 2m_{11}m_{22}{m_{35}}^2 \end{aligned} \tag{29}$$

$$\begin{aligned} a_0 = {} & -2m_{13}m_{35}^3m_{15} - m_{22}m_{13}^2m_{44}^2 + m_{13}^2m_{35}^2m_{44} \\ & + 2m_{13}m_{22}m_{34}m_{14}m_{44} + 2m_{13}m_{22}m_{35}m_{15}m_{44} \\ & + {m_{13}}^2{m_{34}}^2m_{44} - 2m_{11}m_{22}{m_{34}}^2m_{44} \\ & - 2m_{13}{m_{34}}^3m_{14} - 2m_{11}m_{22}{m_{35}}^2m_{44} \\ & + 2m_{11}{m_{35}}^2{m_{34}}^2 + m_{22}{m_{14}}^2{m_{35}}^2 \\ & - 2m_{13}{m_{35}}^2m_{34}m_{14} - 2m_{13}{m_{34}}^2m_{35}m_{15} \\ & + m_{11}{m_{34}}^4 + m_{22}{m_{15}}^2{m_{34}}^2 + m_{22}{m_{35}}^2{m_{15}}^2 \\ & + m_{11}{m_{35}}^4 + m_{11}{m_{22}}^2{m_{44}}^2 + m_{22}{m_{34}}^2{m_{14}}^2 \\ & - {m_{22}}^2{m_{15}}^2m_{44} - {m_{22}}^2{m_{14}}^2m_{44}. \end{aligned} \tag{30}$$

The two candidate values $\lambda^{(1)}, \lambda^{(2)}$ for λ can be found in closed form as the roots of the second-order polynomial; one should examine both candidates, compute the corresponding vectors $\boldsymbol{\varphi}^{(1)}$, $\boldsymbol{\varphi}^{(2)}$, and check which one corresponds to the minimizer of the problem (23).

Let $\lambda^{(i)}$, $i = 1, 2$, be one of the two candidates. The 5×5 matrix $(\boldsymbol{M} + \lambda^{(i)}\boldsymbol{W})$ has rank *at most* 4 by construction. Under the excitability conditions discussed earlier, the rank is guaranteed to be exactly 4. In fact, otherwise, we would be able to find a continuum of solutions for $\boldsymbol{\varphi}$, while the observability analysis guarantees the local uniqueness of the solution.

If the rank is 4, the kernel has dimension 1, and the choice of $\boldsymbol{\varphi}$ is unique given the constraints (8) and (25). Let $\boldsymbol{\gamma}^{(i)}$ be any nonzero vector in the kernel of $\left(\boldsymbol{M} + \lambda^{(i)}\boldsymbol{W}\right)$. To obtain the solution $\boldsymbol{\varphi}^{(i)}$, scale $\boldsymbol{\gamma}^{(i)}$ by $\|(\gamma_4^{(i)}\ \gamma_5^{(i)})^T\|$ to enforce constraint (8), then flip it by the sign of γ_1^i to satisfy constraint (25)

$$\boldsymbol{\varphi}^{(i)} = \frac{\operatorname{sign}(\gamma_1^{(i)})}{\|(\gamma_4^{(i)}\ \gamma_5^{(i)})^T\|}\boldsymbol{\gamma}^{(i)}. \tag{31}$$

The correct solution $\hat{\boldsymbol{\varphi}}$ to (23) can be chosen between $\boldsymbol{\varphi}^{(1)}$ and $\boldsymbol{\varphi}^{(2)}$ by computing the value of the objective function. Given $\hat{\boldsymbol{\varphi}}$ and the previously estimated values of $\hat{J}_{21}, \hat{J}_{22}$, all six parameters can be recovered as follows:

$$\begin{aligned} \hat{b} &= \hat{\varphi}_1 \\ \hat{r}_{\mathrm{L}} &= -\hat{\varphi}_1\hat{J}_{21}, \quad \hat{r}_{\mathrm{R}} = +\hat{\varphi}_1\hat{J}_{22} \\ \hat{\boldsymbol{\ell}} &= (\hat{\varphi}_2, \hat{\varphi}_3, \operatorname{arctan2}(\hat{\varphi}_5, \hat{\varphi}_4)). \end{aligned} \tag{32}$$

C. Outlier Removal

The practicality of the method comes from the fact that one can easily obtain thousands of observations by driving the robot, unattended, along arbitrary trajectories (compare, for example, with Borenstein's method, which is based on precise observation of a small set of data). Unfortunately, within thousands of observations, it is very likely that some are unusable, due to slipping of the wheels, failure of the sensor displacement estimation procedure, and the incorrect synchronization of sensor and odometry observations. In principle, a single outlier can drive the estimate arbitrarily far from the true value; formally, the *breakdown point* of a maximum-likelihood estimator is 0. Thus, we integrate a simple outliers removal procedure, which consists of the classic strategy of progressively discarding a fraction of the samples [33]. For this application, we expect the outliers to be comparatively few with respect to the inliers. If this is the case, a simple trimmed nonlinear optimization is easy to implement and gives good results. Call a *sample* the set of measurements (wheel velocities, estimated sensor displacement) relative to the kth interval. Repeat N times the following:

1) Run the calibration procedure with the current samples.
2) Compute the χ-value of each sample as

$$\chi^k = \|\hat{\boldsymbol{s}}^k - \ominus\hat{\boldsymbol{\ell}} \oplus \boldsymbol{r}^k(\hat{r}_{\mathrm{L}}, \hat{r}_{\mathrm{R}}, \hat{b}) \oplus \hat{\boldsymbol{\ell}}\|_{\boldsymbol{\Sigma}_k^{-1}}. \tag{33}$$

3) Discard a fraction α of samples with highest values of χ^k.

The fraction of samples remaining at the last iteration is $\beta = 1 - (1 - \alpha)^N$. The value of β should be chosen as to underestimate the number of inliers and, thus, depends on the characteristics of the data. The exact values of N and α have less importance as long as the value of β is preserved.

The empirical distribution of the residual errors

$$\boldsymbol{e}^k = \hat{\boldsymbol{s}}^k - \ominus\hat{\boldsymbol{\ell}} \oplus \boldsymbol{r}^k(\hat{r}_{\mathrm{L}}, \hat{r}_{\mathrm{R}}, \hat{b}) \oplus \hat{\boldsymbol{\ell}} \tag{34}$$

gives precious information about the convergence of the estimation procedure. Ideally, if the estimation is accurate, the residuals $\boldsymbol{e}^k$ should be distributed according to the error model of the sensor displacement estimation procedure. For example, Fig. 3 shows the evolution of the residuals in one of the experiments to be presented later. We can see that in the first iteration [see Fig. 3(a)], there are a few outliers; with every iteration, larger outliers are discarded, and because the estimate consequently improves, the residual distribution tends to be Gaussian shaped [see Fig. 3(b)], with x, y errors on the order of millimeters, and θ errors well below 1°.

D. Uncertainty Estimation

The CRB can be used to estimate the uncertainty of the solution. The maximum-likelihood estimator is *asymptotically* unbiased and attains the CRB [31]. If we have thousands of

samples, we expect them to be in the asymptotic regime of the maximum-likelihood estimator. The CRB is computed from the FIM. For an observation model of the kind $\boldsymbol{y}_k = \boldsymbol{f}_k(\boldsymbol{x}) + \boldsymbol{\epsilon}_k$, where $\boldsymbol{f}$ is differentiable, $\boldsymbol{x} \in \mathbb{R}^n$, $\boldsymbol{y} \in \mathbb{R}^m$, and $\boldsymbol{\epsilon}_k$ is Gaussian noise with covariance $\boldsymbol{\Sigma}_k$, the FIM is the $n \times n$ matrix given by $\boldsymbol{\mathcal{I}}(\boldsymbol{x}) = \sum_k \frac{\partial \boldsymbol{f}_k}{\partial \boldsymbol{x}} \boldsymbol{\Sigma}_k^{-1} \frac{\partial \boldsymbol{f}_k}{\partial \boldsymbol{x}}$. Under some technical conditions [31], the CRB states that any unbiased estimator $\hat{\boldsymbol{x}}$ of $\boldsymbol{x}$ is bounded by $\mathrm{cov}(\hat{\boldsymbol{x}}) \geq \boldsymbol{\mathcal{I}}(\boldsymbol{x})^{-1}$. In our case, the observations are $\boldsymbol{y}_k = \hat{\boldsymbol{s}}^k$, the state is $\boldsymbol{x} = (r_{\mathrm{R}}, r_{\mathrm{L}}, b, \ell_x, \ell_y, \ell_\theta)$, and the observation model $\boldsymbol{f}_k$ is given by (8), which is differentiated to obtain $\partial \boldsymbol{f}_k / \partial \boldsymbol{x}$.

E. Simpler Formulas for Constant Wheel Velocities

In Sections V-A and V-B, we needed to integrate the kinematics to obtain some of the coefficients in the optimization problem. If the wheel velocities are constant within the time interval: $v(t) = v_0$, $\omega(t) = \omega_0 \neq 0$, then the solution of (13) can be written in a closed form as

$$\boldsymbol{r}(t) = \begin{pmatrix} (v_0/\omega_0)\sin(\omega_0 t) \\ (v_0/\omega_0)\ (1 - \cos(\omega_0 t)) \\ \omega_0 t \end{pmatrix}. \tag{35}$$

(For a proof, see, for example, [34, p. 516, formula (11.85)].) Let ω_{L}^k, ω_{R}^k be the constant wheel velocities during the kth interval of duration $T^k = t_{k+1} - t_k$. Using (35), (10) can be simplified to

$$\boldsymbol{L}_k = \begin{pmatrix} T^k \omega_{\mathrm{L}}^k & T^k \omega_{\mathrm{R}}^k \end{pmatrix} \tag{36}$$

and (19) and (20) are simplified to

$$r_\theta^k = J_{21} T^k \omega_{\mathrm{L}}^k + J_{22} T^k \omega_{\mathrm{R}}^k \tag{37}$$

$$c_x^k = \tfrac{1}{2} T^k (-J_{21} \omega_{\mathrm{L}}^k + J_{22} \omega_{\mathrm{R}}^k) \frac{\sin(r_\theta^k)}{r_\theta^k} \tag{38}$$

$$c_y^k = \tfrac{1}{2} T^k (-J_{21} \omega_{\mathrm{L}}^k + J_{22} \omega_{\mathrm{R}}^k) \frac{1 - \cos(r_\theta^k)}{r_\theta^k}. \tag{39}$$

Thus, if velocities are constant during each interval, one does not need to evaluate any integral numerically.

1) Bounding the Approximation Error: Assuming constant wheel velocities simplifies the implementation. However, in practice, wheel velocities are never exactly constant. Fortunately, we can characterize precisely the error that we commit if the wheel velocities are not exactly constant. Suppose that we take the nominal trajectory to be generated by the average velocities; for example, we read the odometer at the beginning and the end of the interval, and we divide by the interval length to obtain the average velocities. We obtain

$$\bar{\omega}_{\mathrm{L}} = \frac{1}{T} \int_0^T \omega_{\mathrm{L}}(\tau) d\tau, \quad \bar{\omega}_{\mathrm{R}} = \frac{1}{T} \int_0^T \omega_{\mathrm{R}}(\tau) d\tau.$$

Furthermore, assume that the variation is bounded

$$|\omega_{\mathrm{L}}(t) - \bar{\omega}_{\mathrm{L}}| \leq \epsilon, \quad |\omega_{\mathrm{R}}(t) - \bar{\omega}_{\mathrm{R}}| \leq \epsilon. \tag{40}$$

In these conditions, we can prove the following. First, the approximation constant velocities do not impact the estimation of J_{21}, J_{22}, because the statistics that we need are the total wheel rotations in the interval. Therefore, (10) and (36) coincide, if we use the average velocities as nominal velocities. The constant-velocity approximation does have an impact for the estimation of the other parameters inasmuch as the statistics (19)–(20) are perturbed. Fortunately, this perturbation is bounded by the maximum deviation ϵ. This can be seen by noticing from (18) that the statistics (19)–(20) are proportional to the robot displacement r_x^k, r_y^k. Therefore, their perturbation can be bounded by the maximum perturbation of the nominal unicycle trajectory when the real velocities respect the bounds (40). One can see that the norm of the difference between the nominal trajectory $(\overline{r}_x(t)\ \overline{r}_y(t))^T$ corresponding to the nominal velocities $\bar{\omega}_{\mathrm{L}}, \bar{\omega}_{\mathrm{R}}$ and the real trajectory $(r_x(t)\, r_y(t))^T$ is bounded by $\epsilon\, t$, by imagining two unicycles that start from the same pose and move with different velocities (the worst case is when they travel in opposite directions, in which case the bound $\epsilon\, t$ is exact).

In conclusion, the approximation error derived from assuming constant velocities has no effect on the estimation of J_{12} and J_{22}, and a first-order effect of ϵT on the estimation of the other parameters.

VI. On the Choice of Trajectories

The method does not impose choosing a particular trajectory. This means, for example, that it can be run from logged data, which were not necessarily captured for the purpose of calibration. However, if one is allowed to choose the trajectories explicitly for calibration purposes, then there are a number of relevant considerations, which we discuss in this section. First, we discuss those that are mathematical in nature; then, we discuss the more practical considerations.

A. Mathematical Considerations

Obviously, one should choose commands that make the estimation problem observable. This is not difficult, as we have seen in Section III that the problem is observable if one chooses any two independent trajectories. In principle, we would like to choose the trajectories that are optimal, in the sense that they maximize the information matrix of the parameters that need to be estimated. Unfortunately, we do not have optimality results for all parameters, because of the nonlinearity of the problem.

For the linear part of the problem (estimation of J_{21}, J_{22} in Section V-A), we can completely characterize what are the optimal trajectories. The matrix $\boldsymbol{P}_J^{-1} = \sum_k \boldsymbol{L}_k^T \boldsymbol{L}_k / \left(\sigma_\theta^k\right)^2$ that appears in (11) is the inverse of the covariance matrix for the parameters $\hat{J}_{21}$, $\hat{J}_{22}$. There are several choices for expressing optimality in a statistical sense, which correspond to different functions of the matrix $\boldsymbol{P}_J$. For example, if one wants to minimize the volume of the uncertainty ellipsoid, one should minimize the determinant of $\boldsymbol{P}_J$. Minimizing the trace corresponds to minimizing the expected mean squared error. Assuming the wheel velocities are upper bounded (for example, by the practical considerations below), one can prove that we should choose the trajectories such that the velocities of the two wheels are uncorrelated. This leads to the solution to be a trajectory with alternate tracts of $[+1, -1]$, $[+1, +1]$ (up to sign). Proposition 9

in Appendix C gives a more formal statement and proof of this result.

For the nonlinear part of the analysis, we limit ourselves to more intuitive considerations. It is interesting to notice the following properties of pure motions.[2] A *pure rotation* does not give any information about the wheel axis b and the relative sensor orientation ℓ_θ, while it allows us to observe the distance of the sensor from the robot platform center ($\sqrt{\ell_y^2 + \ell_x^2}$) (see Lemma 16). A *pure translation* does not give any information about ℓ_x and ℓ_y, while it allows us to observe the sensor orientation ℓ_θ directly, as well as the wheel axis b (see Lemma 15).

These results provide a guideline for choosing the calibration trajectories. If the estimation of the sensor orientation ℓ_θ or the wheel axis b is more important than estimating ℓ_x, ℓ_y for the particular application, then use more pure rotations; otherwise, use more pure translations.

B. Practical Considerations

We have seen so far what considerations of optimality suggest for the choice of the trajectories. There are equally important considerations based on more practical aspects.

Obviously, the more the data, the better. Therefore, choosing commands that result in closed trajectories in a small confined space so that the robot can run unattended and obtain a large set of measurements is suggested. Because the dynamics are affine in the parameters, imposing certain wheel velocities $(\omega_{\mathrm{L}}, \omega_{\mathrm{R}})$ for T seconds, and then the opposite velocities $(-\omega_{\mathrm{L}}, -\omega_{\mathrm{R}})$, will move the robot back to the starting point (up to noise), for any parameter configuration. This technique is advised so as to obtain closed trajectories, instead of programming trajectories that close a loop (closing a loop exactly needs previous knowledge of the calibration parameters, which is the principle of UMBmark). One can show that these kinds of trajectories contain the optimal trajectories (see Proposition 14).

With minimal tuning of the maximum velocities and the interval length, one can make the robot stay in a small region. If the exteroceptive sensor is a range-finder, it might be desirable to implement some safety mechanism. In similar situations, we have found the following simple algorithm useful. Define a safety radius for the obstacles; then, if the current motion has led to the safety radius to be violated, interrupt the current commands and send the opposite commands until the robot is in a safe zone. Because the differential-drive dynamics is reversible, this simple algorithm allows the robot to back up into safety without knowing the calibration parameters.

If possible, choose piecewise-constant inputs. This allows us to use the simplified formulas in Section V-E and memorize only one value for ω_{L} and ω_{R} in each interval, instead of memorizing the entire profile $\omega_{\mathrm{L}}(t)$, $\omega_{\mathrm{R}}(t)$ for $t \in [t_k, t_{k+1}]$, which is necessary for using the formulas for the generic case.

Choose commands that lead to relatively low speeds. This minimizes the possibility of slipping and ensures that the sensor data are not perturbed by the robot motion. However, do not choose speeds so low that the nonlinear effects of the dynamics become relevant, especially if using the constant speed assumption (usually robots with DC motors are commanded in velocities via voltage, but the platform does not attain constant velocity instantaneously).

[2]Note that the commands $[+1, -1]$ and $[+1, +1]$ produce a pure rotation and a pure translation, respectively, only if the wheels are of the same radius.

Fig. 2. One Khepera III robot used in the experiments.

VII. Experiments

We tested the method using a Khepera III robot with an on-board Hokuyo URG-04LX range-finder. The software and data logs are available as part of the supplemental materials.

1) Robot: The Khepera III is a small mobile robot suitable for educational use (see Fig. 2). It has a diameter of 13 cm and a weight of 690 g. Brushless servo motors allow a maximum speed of 0.5 m/s. The Khepera III has an encoder resolution of about 7 ticks per degree. The Khepera's on-board CPU (DsPIC 30F5011 60 MHz with the proprietary Korebot extension at 400 MHz) is too slow to perform scan matching in real time because it does not possess a floating point unit. A scan-matching operation that would take about 10 ms on a desktop computer takes about 10 s on the Khepera using floating point emulation. Therefore, the range-finder and odometry measurements are transmitted back to a desktop computer that runs the calibration procedure. Given the scan-matching results $\hat{\boldsymbol{s}}^k$, the computational cost of the calibration algorithm in itself is negligible and can be implemented on the Khepera, even with floating point emulation.

2) Environment: For calibration purposes, it makes sense to use the simplest environment possible, in which the scan-matching operation has the maximum performance. For these experiments, we used a rectangular environment (approximately 1.2 m $\times$ 0.7 m). In this environment, the scan-matching operation can use all readings of the sensor, with no risk of correspondence outliers, and, consequently, achieve the maximum accuracy possible.

3) Sensor: The Hokuyo URG-04LX is a lightweight range-finder sensor [35], [36]. It provides 681 rays over a 240° field of view, with a radial resolution of 1 mm, and a standard deviation of about 3 mm. The measurements are highly correlated, with every ray's error being correlated with its three to four neighbors. This is probably a symptom of some postprocessing (interpolation) to bump up the resolution to the nominal 1024/360 rays/degrees. There is a bias exhibiting temporal drift. Readings change as much as 20 mm over a period of 5 min—this

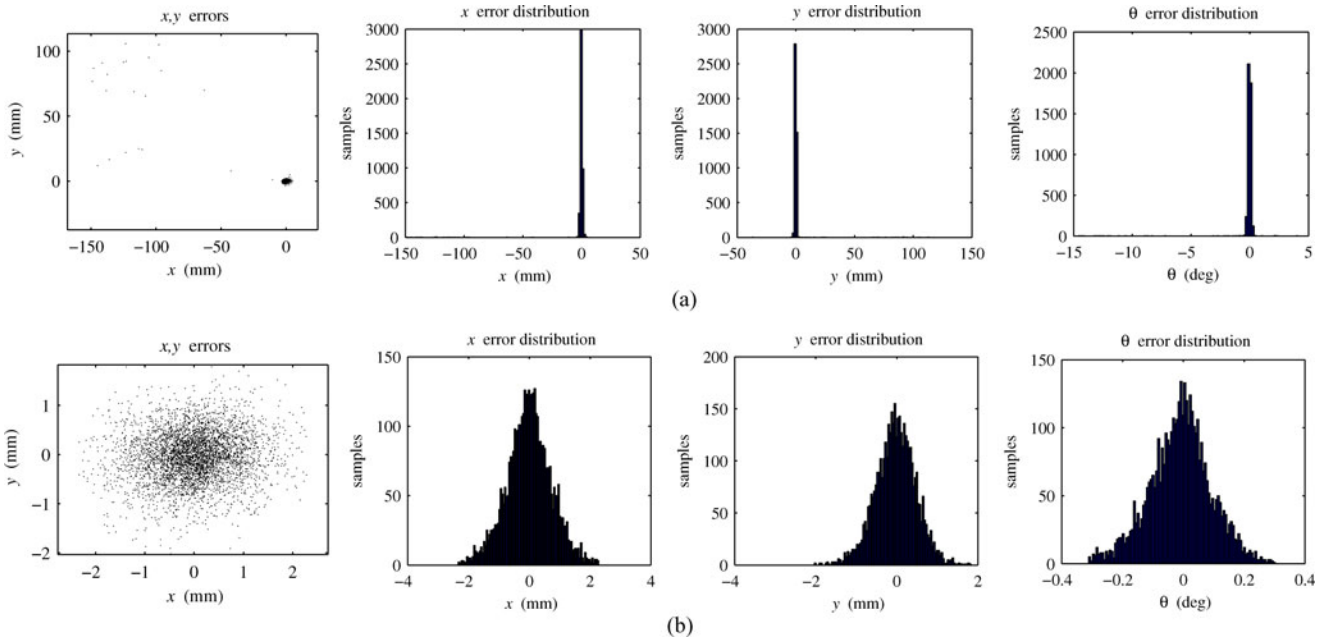

Fig. 3. Residuals distribution after one iteration (top) and after four iterations (bottom). An integral part of the method is the identification and removal of outliers, which may be due to wheel slipping, failure in the sensor displacement estimation procedure, and other unmodeled sources of noise. To identify outliers, one first performs calibration and then computes the residual for each sample, according to (34). Samples with large residuals are discarded and the process is repeated. The distribution of residuals gives information about the quality of the estimate. (a) In the first iteration, we expect large residuals. If the procedure is correct, the residuals should be ultimately distributed according to the sensor model. (b) In this case, we see that at the end of calibration, the residuals are distributed according to the scan-matching error process: approximately Gaussian, with a precision in the order of millimeters and fractions of a degree. (a) Residuals after 1 iteration. (b) Residuals after four iterations.

could be due to the battery power, or the change in temperature. There is also a spatial bias which is a function of the distance [35]. In practice, a rectangular environment appears slightly curved to the sensor. Fortunately, both sources of bias have a negligible effect on this method. Because we only use pairwise scan matching between measurements close in time, the bias (both spatial and temporal) is approximately the same on each range scan and does not impact the scan-matching results. We estimated the results of a scan-matching operation to be accurate in the order of 1 mm and tenths of degrees for small (5–10 cm) displacements.

4) Estimation of Sensor Displacement: We used the scan-matching method described in [37] to obtain the estimates $\hat{\boldsymbol{s}}^k$. There are various possible ways to estimate the covariance $\boldsymbol{\Sigma}_k$: either by using the knowledge of the internal workings of the scan-matching method (see, e.g., [38]) or by using CRB-like bounds [39], which are independent of the algorithm, but assume the knowledge of an analytical model for the sensor.

Alternatively, if the robot has been collecting measurements in a uniform environment so that it is reasonable to approximate the time-variant covariance $\boldsymbol{\Sigma}_k$ by a constant matrix $\boldsymbol{\Sigma}$, one can use the simpler (and more robust) method of identifying $\boldsymbol{\Sigma}$ directly from the data, by computing the covariance matrix of $\boldsymbol{e}^k$, after the solution has been obtained. This estimate is what is used in the following experiments.

5) Data Processing Details: There is a tradeoff involved in the choice of the interval length T. Choosing short intervals is not recommended, as it might make the method too sensitive to unmodeled effects, such as the synchronization of odometry and range readings, and the robot's dynamics. Moreover, the longer each interval, the more information we have about the parameters in one sample. However, the accuracy of the scan-matching procedure decreases with the length T, because a longer time interval implies a larger displacement, which implies less overlapping between scans and, therefore, less correspondences that can constrain the pose. In general, it is reasonable to choose the length of the interval as the longest for which the exteroceptive sensor gives reliable displacement estimates. In our setting, we first chose the maximum wheel speed to be $\simeq$0.5 rad/s ($\simeq$30°/s), which made sure that the robot does not slip on the particular terrain. We recorded range-finder readings at 5 Hz as well as dense odometry readings (at $\simeq$100 Hz). Then, we used only one in four range readings, which corresponds to choosing an interval of $T \simeq 0.8$ s, such that the robot travels approximately 1 cm (in translation) and 20° (in rotation) per interval. These were judged reasonable motions, because, *a posteriori*, the accuracy of the scan matcher on this data, as computed by the residuals, is in the order of $\sigma_{xy} = 0.3$ mm and $\sigma_\theta = 0.1°$. Each range-finder reading was matched to the closest odometry reading using the recorded timestamp. It was assumed that the wheel velocities were constant in every interval, as previously discussed.

6) Range-Finder Configurations: To test the method, we tried three configurations for the range-finder pose on the same robot. This allows us to check that the estimate for the odometry parameters remains consistent for a different configuration of the laser. We labeled the three configurations A, B, and C.

7) Trajectories: In the experiments, we drive the robot according to trajectories that contain an equal number of the

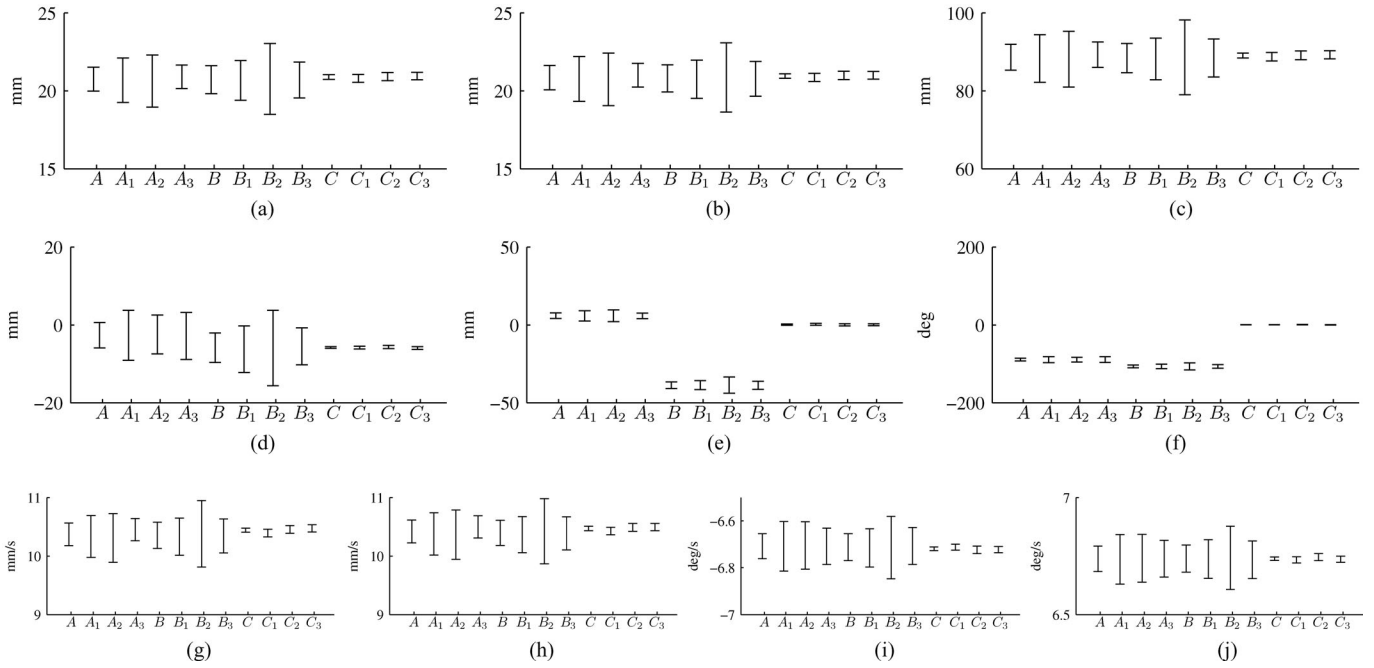

Fig. 4. Calibrated parameters and confidence intervals (the same information is presented in a tabular form in Table II). For each configuration, three logs are taken and considered separately (for example, A_1,A_2,A_3) and all together ("A"). Thus, we have 12 datasets in total. On the x-axis, we find the experiment label and on the y-axis, we find the estimated value, along with 3σ confidence bars. The confidence bars correspond to the absolute achievable accuracy as computed by the CRB, as explained in Section V-D. Note that most variables are highly correlated; therefore, plotting only the standard deviations might be misleading (see Fig. 5 for more information about the correlation). (a) r_{L}. (b) r_{R}. (c) b. (d) ℓ_x. (e) ℓ_y. (f) ℓ_θ. (g) J_{11}. (h) J_{12}. (i) J_{21}. (j) J_{22}.

four pairs of "canonical" inputs $(\omega_{\mathrm{L}}, \omega_{\mathrm{R}}) = \pm\omega_{\max}(+1, +1)$, $\pm\omega_{\max}(+1, -1), \pm\omega_{\max}(+1, 0), \pm\omega_{\max}(0, +1)$. The nominal trajectories that are associated with these inputs are elementary, if the wheels can be assumed to be approximately of the same radius. In particular, the first input corresponds to a straight trajectory; the second to the robot turning in place; and the last two to the motions originated by moving only one wheel. These trajectories are pieced together such that, at the end of each execution, the robot returns to the starting pose (up to drift); in this way, it is possible for the calibration procedure to run unattended in a confined space.

A. Results

For each of the configurations A, B, and C, we collected several data logs using the aforementioned inputs. We divided the data for each configuration into three subsets, which are named A_1, A_2, A_3, B_1, B_2, B_3, and C_1, C_2, C_3, by selecting every third tuple from the main datasets. In this way, we had three independent datasets for each configuration. This division is just for the sake of a proper statistical analysis and is not part of the method. Each subset was composed of about 3500 measurement samples.

For each configuration, we ran the calibration algorithm both on the complete dataset and on each subset individually. Considering multiple subsets for the same configuration allows us to check whether the uncertainty estimate is consistent. For example, we expect that the subsets A_1 and A_2 give slightly different calibration results, but those results must not disagree more than the estimated confidence bounds predict.

The results of calibration for the parameters are shown in Fig. 4. Fig 4(a)–(f) shows the estimates for the parameters r_{R}, r_{L}, b, ℓ_x, ℓ_y, ℓ_θ. Fig. 4(g)–(j) shows the same for the parameters J_{11}, J_{12}, J_{21}, J_{22}. The error bars correspond to the confidence values of 3σ given by the computation of the CRB. Table II contains the data in textual form.

The results are robust to the choice of the outlier rejection parameters. If the actual error distribution is a monomodal distribution (inliers) superimposed with a few samples of a larger-variance distribution (outliers), then the particular choices of α and N do not impact the estimate as long as the final fraction of measurements considered $\beta = 1 - (1 - \alpha)^N$ remains constant [33]. The results in Table II are obtained with $\alpha = 0.01$ and $N = 4$, corresponding to $\beta \simeq 96\%$ of inliers. As an example, we chose $\alpha = 0.005$ and $N = 8$, for which also $\beta \simeq 96\%$. The ratio of the parameters obtained in the two cases is equal to 1 to several decimal places [3] (see Table IV).

1) Comparison to Manually Measured Parameters and UMBmark: The precision of the method is in the order of millimeters and tenths of degrees for the pose of the laser. It is not possible for us to measure ground truth with such precision. For the odometry parameters, we can rely on the nominal specifications for the robot platform, which are $r_{\mathrm{L}} = r_{\mathrm{R}} = 21$ mm and $b = 90$ mm, as well as an alternative calibration method. Our method estimates, for the dataset with less uncertainty (Table II, row "C"), that $r_{\mathrm{L}} = 20.89 \pm 0.05$ mm, $r_{\mathrm{R}} = 20.95 \pm 0.05$ mm,

[3]One exception, highlighted in bold, is the value of ℓ_y for the dataset C_2, for which the ratio is $\simeq$0.71. For that parameter, the confidence interval is estimated as -0.03 ± 0.20 mm (see Table II). The ratio is more variable because the noise is much larger than the absolute value of the mean.

TABLE II
CALIBRATED PARAMETERS AND CONFIDENCE INTERVALS

	r_{L} (mm)	r_{R} (mm)	b (mm)	ℓ_x (mm)	ℓ_y (mm)	ℓ_θ (deg)	J_{11} (mm/s)	J_{12} (mm/s)	J_{21} (deg/s)	J_{22} (deg/s)
A	20.74 ± 0.26	20.84 ± 0.26	88.60 ± 1.10	-2.65 ± 1.09	5.79 ± 0.59	-89.08 ± 1.31	10.37 ± 0.06	10.42 ± 0.07	-6.71 ± 0.02	6.74 ± 0.02
A_1	20.67 ± 0.48	20.76 ± 0.48	88.29 ± 2.04	-2.66 ± 2.14	5.77 ± 1.10	-89.25 ± 2.60	10.34 ± 0.12	10.38 ± 0.12	-6.71 ± 0.04	6.74 ± 0.04
A_2	20.62 ± 0.56	20.73 ± 0.56	88.10 ± 2.39	-2.46 ± 1.66	5.88 ± 1.27	-89.24 ± 2.02	10.31 ± 0.14	10.37 ± 0.14	-6.70 ± 0.03	6.74 ± 0.03
A_3	20.91 ± 0.25	21.00 ± 0.25	89.28 ± 1.08	-2.86 ± 2.01	5.71 ± 0.59	-88.79 ± 2.48	10.45 ± 0.06	10.50 ± 0.06	-6.71 ± 0.03	6.74 ± 0.03
B	20.71 ± 0.30	20.79 ± 0.29	88.39 ± 1.25	-5.87 ± 1.26	-38.71 ± 0.67	-106.58 ± 1.20	10.36 ± 0.07	10.40 ± 0.07	-6.71 ± 0.02	6.74 ± 0.02
B_1	20.67 ± 0.42	20.74 ± 0.41	88.17 ± 1.78	-6.21 ± 1.99	-38.66 ± 0.96	-106.77 ± 1.90	10.33 ± 0.11	10.37 ± 0.10	-6.71 ± 0.03	6.74 ± 0.03
B_2	20.76 ± 0.76	20.85 ± 0.74	88.60 ± 3.20	-5.96 ± 3.23	-38.71 ± 1.73	-106.59 ± 3.05	10.38 ± 0.19	10.43 ± 0.19	-6.71 ± 0.04	6.74 ± 0.04
B_3	20.69 ± 0.39	20.78 ± 0.37	88.39 ± 1.62	-5.51 ± 1.58	-38.78 ± 0.87	-106.37 ± 1.50	10.35 ± 0.10	10.39 ± 0.09	-6.71 ± 0.03	6.73 ± 0.03
C	20.89 ± 0.05	20.95 ± 0.05	89.05 ± 0.21	-5.81 ± 0.08	0.19 ± 0.11	0.54 ± 0.09	10.44 ± 0.01	10.47 ± 0.01	-6.72 ± 0.00	6.74 ± 0.00
C_1	20.79 ± 0.09	20.86 ± 0.09	88.73 ± 0.37	-5.83 ± 0.13	0.37 ± 0.20	0.57 ± 0.16	10.39 ± 0.02	10.43 ± 0.02	-6.71 ± 0.00	6.73 ± 0.00
C_2	20.91 ± 0.09	20.98 ± 0.09	89.11 ± 0.38	-5.70 ± 0.14	-0.03 ± 0.20	0.67 ± 0.16	10.46 ± 0.02	10.49 ± 0.02	-6.72 ± 0.01	6.75 ± 0.01
C_3	20.95 ± 0.08	20.99 ± 0.08	89.27 ± 0.35	-5.95 ± 0.12	0.10 ± 0.19	0.37 ± 0.15	10.47 ± 0.02	10.50 ± 0.02	-6.72 ± 0.00	6.74 ± 0.00

The same information is presented in a graphical form in Fig. 4.

TABLE III
CALIBRATION RESULTS USING UMBMARK

	b (m)	r_{L} (m)	r_{R} (m)	E_b	E_d	$E_{\max}$	J_{11} (m/s)	J_{12} (m/s)	J_{21} (rad/s)	J_{22} (rad/s)
nominal	0.090	0.021	0.021	1.0	1.0	17.8238	0.0105	0.0105	-0.23333	0.23333
after 1 trial	0.08971	0.02100	0.02099	0.996854	0.99963	8.1993	0.010501	0.01050	-0.23411	0.23403
after 2 trials	0.08970	0.02101	0.02099	0.996722	0.99883	6.5975	0.010506	0.01049	-0.23424	0.23396
after 3 trials	0.08965	0.02102	0.02098	0.996180	0.99848	4.4295	0.010507	0.01049	-0.23441	0.23405
after 4 trials	0.08962	0.02101	0.02099	0.995824	0.99868	3.8147	0.010506	0.01049	-0.23447	0.23416

TABLE IV
RATIO OF ESTIMATED PARAMETERS FOR DIFFERENT OUTLIER REJECTION PARAMETERS

	r_{L} ratio	r_{R} ratio	b ratio	ℓ_x ratio	ℓ_y ratio	ℓ_θ ratio	J_{11} ratio	J_{12} ratio	J_{21} ratio	J_{22} ratio
A	1.00001	1.00005	0.99999	0.99135	1.00347	1.00004	1.00001	1.00005	1.00003	1.00006
A_1	0.99998	1.00000	0.99998	1.01479	0.99886	1.00019	0.99998	1.00000	1.00000	1.00003
A_2	0.99986	0.99986	0.99998	0.99074	0.99855	1.00004	0.99986	0.99986	0.99988	0.99988
A_3	1.00000	1.00000	0.99997	1.01434	1.00405	1.00004	1.00000	1.00000	1.00003	1.00003
B	1.00036	1.00029	1.00014	0.99216	0.99930	1.00011	1.00036	1.00029	1.00021	1.00015
B_1	1.00000	1.00000	1.00011	1.00307	0.99954	0.99999	1.00000	1.00000	0.99989	0.99989
B_2	1.00000	1.00000	1.00000	1.00000	1.00000	1.00000	1.00000	1.00000	1.00000	1.00000
B_3	0.99994	0.99999	0.99997	0.99152	1.00051	1.00001	0.99994	0.99999	0.99997	1.00002
C	1.00004	1.00006	1.00006	0.99902	1.00200	1.00358	1.00004	1.00006	0.99998	1.00001
C_1	0.99947	0.99945	0.99942	1.00470	0.97054	0.99850	0.99947	0.99945	1.00005	1.00004
C_2	1.00022	1.00024	1.00034	0.99608	0.71784	0.99223	1.00022	1.00024	0.99988	0.99990
C_3	1.00081	1.00083	1.00087	1.00038	0.93306	0.96520	1.00081	1.00083	0.99994	0.99996

$\alpha = 0.005$, $N = 8$ versus $\alpha = 0.01$ and $N = 4$.

and $b = 89.05 \pm 0.21$ mm. For the direction ℓ_θ of the range-finder, the values are compatible with what we could measure manually. For the A configuration, we had tried to mount it at 90° with respect to the robot orientation, and we obtain $\ell_\theta = -89.08 \pm 1.31°$. For the C configuration, the range-finder was mounted aligned with the robot, and we obtained the estimate $\ell_\theta = 0.54 \pm 0.09°$.

We also calibrated this robot using the UMBmark method, using a ceiling-mounted camera as the external sensor. The camera observes the position and angular orientation in the plane of an artificial marker placed on top of the robot. The UMBmark method was initialized using the nominal specifications ($r_{\mathrm{L}} = r_{\mathrm{R}} = 21$ mm and $b = 90$ mm). After four runs, the UMBmark result for the wheel axis was a correction of $b = 89.62$ mm, which is lower than the initial estimate, in the same direction as our estimate (see Table III). UMBmark slightly adjusted the radii ratio to 0.99868, which is a value that is statistically compatible with our confidence intervals. Finally, the UMBmark method maintains the average of the wheel radii constant, in this case 21 mm. We conclude that our method can obtain accurate results for the odometry that are compatible with the ground truth and established calibration methods.

2) Interdataset Comparison: We cannot measure the exact origin of the range reading (ℓ_x, ℓ_y) with a precision comparable with the method accuracy, because the origin of the range finder is a point housed in an opaque compartment. Yet, we can make the claim that the performance is very close to optimality using an indirect verification: by processing the different subsets of the same log, and verifying that the results agree on the level of confidence given by the associated CRB. For example, Fig. 4 shows that although the estimates of r_{L} are different across the sets A_1, A_2, A_3, they are compatible with the confidence bounds. In the same way, we can compare the estimates for ℓ_x, ℓ_y, ℓ_θ across each configuration. Moreover, the estimates of the odometry

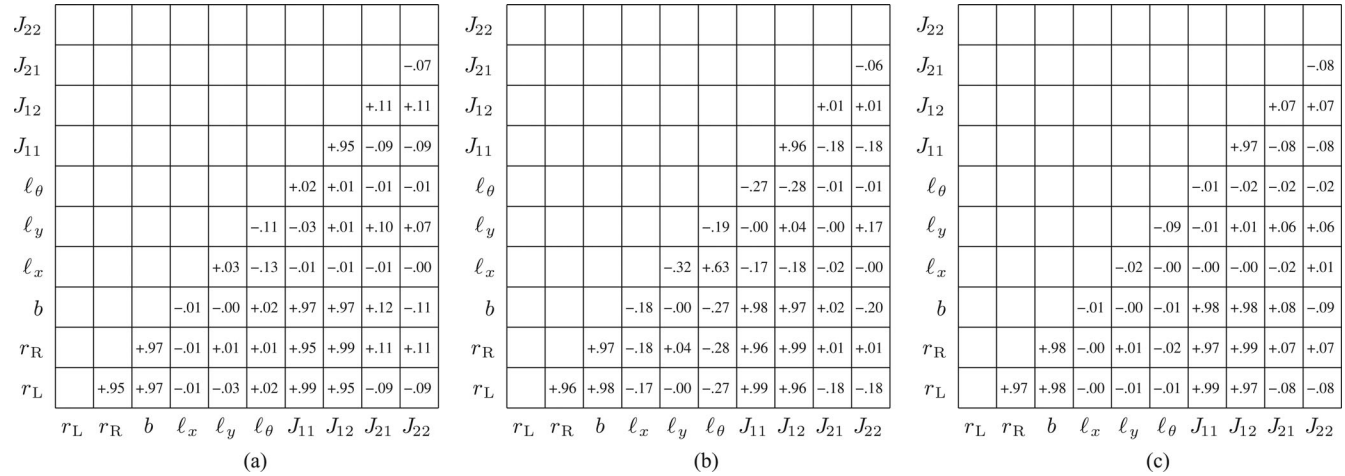

Fig. 5. Correlation patterns between estimation errors. Fig. 4 shows the confidence intervals as 3σ error bars on each variable, which corresponds to considering only the diagonal elements of the covariance matrix and neglecting the correlation information. As it turns out, each configuration has a typical correlation pattern, which critically describes the overall accuracy. (a)–(c) Correlation patterns for the three configurations A, B, C. Each cell in the grid contains the correlation between the two variables on the axes.

parameters r_{R}, r_{L}, and b (and the equivalent parametrization J_{11}, J_{12}, J_{21}, J_{22}) can also be compared across all three configurations A, B, and C. For example, in Fig. 4(g)–(j), we can see that although the estimates of J_{11}, J_{12}, J_{21}, J_{22} change in each set, and the uncertainty varies much as well, all the data are coherent with the level of confidence given by the CRB.

Another confirmation of the accuracy of the method is the distribution of the residuals [see Fig. 3(b)], which is approximately Gaussian and coincides with the scan-matching error model.

3) Correlation Patterns: Note that the uncertainty (error bars) varies considerably across configurations, even though the number of measurements is roughly the same for each set. To explain this apparent inconsistency, one should recall that the confidence limits for a single variable give only a partial idea of the estimation accuracy; in fact, it is equivalent to considering only the diagonal entries of the covariance matrix and neglecting the information about the correlation among variables. For example, the estimates of r_{L} and b are strongly positively correlated, because it is their ratio $J_{21} = r_{\mathrm{L}}/b$ that is directly observable. In this case, there is a large correlation among the variables, and the correlation is influenced by the sensor pose configuration. This is shown in detail in Fig. 5, where the correlation patterns among all variables are presented. In Fig. 5(b), we can see that having a displaced sensor introduces a strong correlation between ℓ_x, ℓ_y, and ℓ_θ. Comparing Fig. 5(a) and (c), we see that simply rotating the sensor does not change the correlation pattern.

VIII. Conclusion

In this paper, we have presented a simple and practical method for simultaneously calibrating the odometric parameters of a differential-drive robot and the extrinsic pose of an exteroceptive sensor placed on the robot. The method has some interesting characteristics. It can run unattended, with no human intervention; no apparatus has to be calibrated *a priori*; there is no need for nominal parameters as an initial guess, as the globally optimal solution is found in a closed form; and robot trajectories can be freely chosen, as long as they excite all parameters. We have experimentally evaluated the method on a mobile platform equipped with a laser range-finder placed in various configurations, using scan matching as the sensor displacement estimation method, and we have showed that the calibration accuracy is comparable with the theoretical limit given by the CRB.

Among the possible evolutions of this study, we mention the simultaneous calibration problem for other kinematic models of mobile platforms, such as the car-like robot. We have assumed that the sensor orientation is planar, yet it would be interesting to consider the case where the sensor is tilted at an arbitrary angle, as is sometimes the case. Another interesting extension would be moving the problem to a dynamic setting, with a sensor that measures forces or accelerations.

Appendix A

Proof of Proposition 2

We want to prove that the two sets of calibration parameters $(r_{\mathrm{L}}, r_{\mathrm{R}}, b, \ell_x, \ell_y, \ell_\theta)$ and $(-r_{\mathrm{L}}, -r_{\mathrm{R}}, -b, -\ell_x, -\ell_y, \ell_\theta + \pi)$ are indistinguishable. We show that this is true because they produce the same sensor velocity and, consequently, the same sensor displacement $\boldsymbol{s}^k$. Denote the sensor velocity in the sensor frame by $\boldsymbol{\nu} = (\nu_x, \nu_y, \nu_\theta) \in \mathrm{se}(2)$, which can be written as

$$\begin{pmatrix} \nu_x \\ \nu_y \end{pmatrix} = \boldsymbol{R}(-\ell_\theta)\left[\begin{pmatrix} v \\ 0 \end{pmatrix} + \begin{pmatrix} 0 & \omega \\ -\omega & 0 \end{pmatrix}\begin{pmatrix} \ell_x \\ \ell_y \end{pmatrix}\right]$$
$$\nu_\theta = \omega. \tag{41}$$

The transformation $r_{\mathrm{L}} \mapsto -r_{\mathrm{L}}, r_{\mathrm{R}} \mapsto -r_{\mathrm{R}}, b \mapsto -b, \ell_\theta \mapsto \ell_\theta + \pi$, $\ell_y \mapsto +\ell_x, \ell_x \mapsto -\ell_y$ leads to the following mappings:

$$\omega \mapsto \omega, \quad \text{(unchanged)}$$
$$v \mapsto -v$$
$$\boldsymbol{R}(-\ell_\theta) \mapsto -\boldsymbol{R}(-\ell_\theta).$$

Substituting these into (41) shows that the sensor velocity is invariant to the transformation.

APPENDIX B

PROOF OF PROPOSITION 3

From the discussion in Section V, we already know that under the conditions of the statement, the parameters J_{21}, J_{22} are observable. We also know that we can estimate r_x^k, r_y^k up to a constant, given by the axis length b; i.e., we can write

$$r_x^k = c_x^k b, \quad r_y^k = c_x^k b$$

where c_1^k and c_2^k are observable constants. What is missing is establishing under what conditions the remaining parameters b and $\boldsymbol{\ell} = (\ell_x, \ell_y, \ell_\theta)$ are observable. The following lemma establishes necessary and sufficient conditions for the parameters to be observable from the observations from two intervals.

Lemma 6: Given the observations from two intervals, in which the relative robot motion was, respectively

$$\boldsymbol{r}^1 = (r_x^1, r_y^1, r_\theta^1), \quad \boldsymbol{r}^2 = (r_x^2, r_y^2, r_\theta^2) \tag{42}$$

and for which, consequently, the relative sensor motion was

$$\boldsymbol{s}^1 = (s_x^1, s_y^1, s_\theta^1), \quad \boldsymbol{s}^2 = (s_x^2, s_y^2, s_\theta^2)$$

the wheel axis b and the sensor pose $\boldsymbol{\ell}$ are observable if and only if the following 4×5 matrix has rank 4:

$$\boldsymbol{M} = \begin{pmatrix} -r_x^1/b & 1-\cos s_\theta^1 & +\sin s_\theta^1 & +s_x^1 & -s_y^1 \\ -r_y^1/b & -\sin s_\theta^1 & 1-\cos s_\theta^1 & +s_y^1 & +s_x^1 \\ -r_x^2/b & 1-\cos s_\theta^2 & +\sin s_\theta^2 & +s_x^2 & -s_y^2 \\ -r_y^2/b & -\sin s_\theta^2 & 1-\cos s_\theta^2 & +s_y^2 & +s_x^2 \end{pmatrix}. \tag{43}$$

Proof: From the vector part of $\boldsymbol{\ell} \oplus \boldsymbol{s}^k = \boldsymbol{r}^k \oplus \boldsymbol{\ell}$, we obtain

$$\boldsymbol{R}(\ell_\theta) \begin{pmatrix} s_x^k \\ s_y^k \end{pmatrix} + \begin{pmatrix} \ell_x \\ \ell_y \end{pmatrix} = \boldsymbol{R}(r_\theta^k) \begin{pmatrix} \ell_x \\ \ell_y \end{pmatrix} + \begin{pmatrix} r_x^k \\ r_y^k \end{pmatrix}.$$

By substituting (18), letting $r_\theta^k = s_\theta^k$, arranging the unknown terms in a vector $\boldsymbol{\varphi}$, given by (21), this is a linear constraint

$$\begin{pmatrix} -c_x^k & 1-\cos s_\theta^k & +\sin s_\theta^k & +s_x^k & -s_y^k \\ -c_y^k & -\sin s_\theta^k & 1-\cos s_\theta^k & +s_y^k & +s_x^k \end{pmatrix} \boldsymbol{\varphi} = \boldsymbol{0}. \tag{44}$$

Note that we are treating $\cos \ell_\theta$ and $\sin \ell_\theta$ as two independent variables, but, of course, we have the constraint $\cos^2 \ell_\theta + \sin^2 \ell_\theta = 1$. The constraints derived by two intervals can be considered together by stacking two copies of (44)

$$\begin{pmatrix} -c_x^1 & 1-\cos s_\theta^1 & +\sin s_\theta^1 & +s_x^1 & -s_y^1 \\ -c_y^1 & -\sin s_\theta^1 & 1-\cos s_\theta^1 & +s_y^1 & +s_x^1 \\ -c_x^2 & 1-\cos s_\theta^2 & +\sin s_\theta^2 & +s_x^2 & -s_y^2 \\ -c_y^2 & -\sin s_\theta^2 & 1-\cos s_\theta^2 & +s_y^2 & +s_x^2 \end{pmatrix} \boldsymbol{\varphi} = \boldsymbol{0}.$$

This is a homogeneous linear system of the kind $\boldsymbol{M}\boldsymbol{\varphi} = 0$, where $\boldsymbol{M}$ can be written as in (43). Note that there are five unknowns and four constraints: $\boldsymbol{\varphi} \in \mathbb{R}^5$ and $\boldsymbol{M} \in \mathbb{R}^{4\times 5}$; therefore, considering only the linear system $\boldsymbol{M}\boldsymbol{\varphi} = 0$, the vector $\boldsymbol{\varphi}$ can be observed only up to a subspace of dimension 1 ($\ker M$): if $\boldsymbol{\varphi}$ is a solution, also $\alpha\boldsymbol{\varphi}$ is a solution, for any $\alpha \in \mathbb{R}$.

The additional constraints (24)–(25) allow us to determine the solution uniquely. The absolute value of $\boldsymbol{\varphi}$ is constrained by (24). There is still a sign ambiguity, which corresponds to the representation ambiguity of Proposition 2. The sign is found using the convention that $b = \varphi_1 > 0$ (thus giving b the physical interpretation of a distance). In conclusion, the vector $\boldsymbol{\varphi}$ is observable if and only if $\boldsymbol{M}$ has rank 4. ∎

The next question is clearly for which trajectories the matrix $\boldsymbol{M}$ in (43) has rank 4. First, notice that $\boldsymbol{M}$ depends only on the relative robot displacement at the end of the interval, i.e., on the vectors $\boldsymbol{r}^1$ and $\boldsymbol{r}^2$ in (42), as well as on the relative sensor displacements $\boldsymbol{s}^1$ and $\boldsymbol{s}^2$, which are a function of $\boldsymbol{r}^1$ and $\boldsymbol{r}^2$, assuming $\boldsymbol{\ell}$ fixed. In other words, the observability of the parameters depend only on the final pose of the robot at the end of the intervals, but not on *how* the robot arrived there. In particular, it does not matter whether the robot velocities were constant or variable in time.

Proposition 7: Let $\mathrm{Log} : \mathrm{SE}(2) \to \mathrm{se}(2)$ be the logarithmic map on $\mathrm{SE}(2)$. Then, the matrix $\boldsymbol{M}$ has rank less than 4 if and only if 1) both $\boldsymbol{s}^1$ and $\boldsymbol{s}^2$ are pure translations, or 2) there exists a $\gamma \in \mathbb{R}$ such that

$$\mathrm{Log}(\boldsymbol{s}^1) = \gamma\, \mathrm{Log}(\boldsymbol{s}^2). \tag{45}$$

Proof: Let us first consider the case in which one of the trajectories is a pure translation. Without loss of generality, let $s_\theta^1 = 0$. Also assume that either s_x^1 or s_y^1 is nonzero, because, if $\boldsymbol{s}^1$ is the zero motion, then the problem is unobservable, and the proposition holds by choosing $\gamma = 0$ in (45). If $s_\theta^1 = 0$, then $r_x^1 = s_x^1$ and $r_y^1 = s_y^1$, because sensor and robot saw exactly the same total motion. In this case, the matrix $\boldsymbol{M}$ is

$$\begin{pmatrix} -\left(\frac{1}{b}\right) s_x^1 & 0 & 0 & +s_x^1 & -s_y^1 \\ -\left(\frac{1}{b}\right) s_y^1 & 0 & 0 & +s_y^1 & +s_x^1 \\ -r_x^2/b & 1-\cos s_\theta^2 & +\sin s_\theta^2 & +s_x^2 & -s_y^2 \\ -r_y^2/b & -\sin s_\theta^2 & 1-\cos s_\theta^2 & +s_y^2 & +s_x^2 \end{pmatrix}. \tag{46}$$

If also the second trajectory corresponds to a pure translation ($s_\theta^2 = 0$), then this matrix has rank at most 2, because the second and third columns are zero, and the first column is a multiple of the fourth. For two pure translations, the parameters are unobservable. If the second trajectory is not a pure translation ($s_\theta^2 \neq 0$), then the matrix $\boldsymbol{M}$ has rank 4, as can be seen by looking at the determinant of the 4×4 minor

$$\begin{pmatrix} 0 & 0 & +s_x^1 & -s_y^1 \\ 0 & 0 & +s_y^1 & +s_x^1 \\ 1-\cos s_\theta^2 & +\sin s_\theta^2 & +s_x^2 & -s_y^2 \\ -\sin s_\theta^2 & 1-\cos s_\theta^2 & +s_y^2 & +s_x^2 \end{pmatrix}$$

which is $2(\cos(s_\theta^2) - 1)\|(s_x^1 \; s_y^1)^T\|^2 \neq 0$. Let us now discuss the general case, in which none of the trajectories is a pure translation: $(\omega_1, \omega_2 \neq 0)$. Write the poses $\boldsymbol{s}^1$, $\boldsymbol{s}^2$ using the

exponential coordinates (a_1, b_1, ω_1) and (a_2, b_2, ω_2)

$$\mathrm{Log}(\boldsymbol{s}^k) = T \begin{pmatrix} 0 & \omega_k & a_1 \\ -\omega_k & 0 & b_k \\ 0 & 0 & 0 \end{pmatrix} \in \mathrm{se}(2)$$

for $a_k, b_k \in \mathbb{R}$ and ω_k such that $|\omega_i| < \pi/T$. This last constraint, corresponding to $|\omega_i T| < \pi$, ensures that this is a one-to-one reparametrization of the data.

The vectors (a_1, b_1, ω_1) and (a_2, b_2, ω_2) have the interpretation of the constant velocities that would give the two final poses in time T; however, notice that this is just a parametrization of the data $\boldsymbol{s}^1$ and $\boldsymbol{s}^2$; there is no assumption on the velocities actually being constant during the interval.

We need to show that the matrix $\boldsymbol{M}$ has rank less than 4 if and only if there exists a $\gamma \in \mathbb{R}$ such that

$$(a_2\ b_2\ \omega_2)^T = \gamma (a_1\ b_1\ \omega_1)^T. \tag{47}$$

Lemma 8 gives the closed-form expression for the coordinates $(s_x^k, s_y^k, s_\theta^k)$, which appear in (50) as a function of the exponential coordinates (a_k, b_k, ω_k)

$$s_\theta^k = \omega_k T \tag{48}$$

$$\begin{aligned} \begin{pmatrix} s_x^k \\ s_y^k \end{pmatrix} &= \begin{pmatrix} \dfrac{\sin(\omega_k T)}{\omega_k T} & \dfrac{\cos(\omega_k T) - 1}{\omega_k T} \\ \dfrac{1 - \cos(\omega_k T)}{\omega_k T} & \dfrac{\sin(\omega_k T)}{\omega_k T} \end{pmatrix} \begin{pmatrix} a_k T \\ b_k T \end{pmatrix} \\ &= \frac{1}{\omega_k} \begin{pmatrix} \sin(\omega_k T) & \cos(\omega_k T) - 1 \\ 1 - \cos(\omega_k T) & \sin(\omega_k T) \end{pmatrix} \begin{pmatrix} a_k \\ b_k \end{pmatrix}. \end{aligned} \tag{49}$$

Consider again the 4×4 minor of $\boldsymbol{M}$ corresponding to the last four columns

$$\tilde{\boldsymbol{M}} = \begin{pmatrix} 1 - \cos s_\theta^1 & +\sin s_\theta^1 & +s_x^1 & -s_y^1 \\ -\sin s_\theta^1 & 1 - \cos s_\theta^1 & +s_y^1 & +s_x^1 \\ 1 - \cos s_\theta^2 & +\sin s_\theta^2 & +s_x^2 & -s_y^2 \\ -\sin s_\theta^2 & 1 - \cos s_\theta^2 & +s_y^2 & +s_x^2 \end{pmatrix}. \tag{50}$$

Substitute (48) and (49) into (50) to obtain the matrix $\tilde{\boldsymbol{M}}$ as a function of only the exponential coordinates (a_k, b_k, ω_k). The determinant of $\tilde{\boldsymbol{M}}$ can be computed as

$$\begin{aligned} \det \tilde{\boldsymbol{M}} = T^3 \mathrm{sinc}^2\,(\omega_1 T/2)\, \mathrm{sinc}^2\,(\omega_2 T/2)\, ((a_2^2 + b_2^2)\omega_1^2 \\ - 2(a_1 a_2 + b_1 b_2)\omega_1 \omega_2 + (a_1^2 + b_1^2)\omega_2^2). \end{aligned}$$

The zeros of $\mathrm{sinc}(x)$ are the same zeros as $\sin(x)$ (except $x = 0$, as $\mathrm{sinc}(0) = 1$); hence, the determinant is zero for $\omega_i T/2 = k\pi$ ($|k| > 0$), but these zeros can be ignored as they correspond to $\omega_i T = 2k\pi$, which are singularities of the representation. In fact, we had already assumed that $|\omega_i T| < \pi$. Therefore, the determinant is 0 if and only if the second factor

$$d = (a_2^2 + b_2^2)\omega_1^2 - 2(a_1 a_2 + b_1 b_2)\omega_1 \omega_2 + (a_1^2 + b_1^2)\omega_2^2 \tag{51}$$

is equal to 0. This is a polynomial of the fourth order in the variables (a_1, b_1, ω_1) and (a_2, b_2, ω_2). It is also a homogeneous polynomial (all summands have the same order), which is a clue that it might be further simplified. We discuss four cases.

1) If the trajectory is a pure rotation ($a_1, b_1 = 0$), then $d = (a_2^2 + b_2^2)\omega_1^2$, which is nonzero as long as the second motion is not also a pure rotation.

2) If both coordinates are nonzero ($a_1, b_1 \neq 0$), we can reparametrize (a_2, b_2, ω_2) using the three numbers $(\alpha, \beta, \gamma) \in \mathbb{R}^3$, according to this particular transformation

$$a_2 = (\alpha\gamma) a_1, \quad b_2 = (\beta\gamma) b_1, \quad \omega_2 = (\gamma)\omega_1.$$

Because $\omega_1, \omega_2 \neq 0$, necessarily $\gamma \neq 0$. Substituting these into (51), we obtain

$$\begin{aligned} d &= (\alpha^2\gamma^2 a_1^2 + \beta^2\gamma^2 b_1^2)\omega_1^2 - 2(\alpha\gamma a_1^2 + \gamma\beta b_1^2)\gamma\omega_1^2 \\ &\quad + (a_1^2 + b_1^2)\gamma^2\omega_1^2 \\ &= (\gamma^2\omega_1^2)\left(\alpha^2 a_1^2 + \beta^2 b_1^2 - 2(\alpha a_1^2 + \beta b_1^2) + a_1^2 + b_1^2\right) \\ &= (\gamma^2\omega_1^2)\left((\alpha^2 - 2\alpha + 1)a_1^2 + (\beta^2 - 2\beta + 1)b_1^2\right) \\ &= (\gamma^2\omega_1^2)\left((\alpha - 1)^2 a_1^2 + (\beta - 1)^2 b_1^2\right). \end{aligned}$$

Therefore, the determinant is zero if and only if $\alpha = 1$ and $\beta = 1$, in which case it holds that (a_2, b_2, ω_2) is proportional to (a_1, b_1, ω_1) by the constant γ.

3) If $a_1 = 0$ and $b_1 \neq 0$, we need to use a simpler variation of the proof for the previous case. In this case, use the parametrization (x, β, γ), such that $a_2 = \gamma x$, $b_2 = (\beta\gamma) b_1$ and $\omega_2 = (\gamma)\omega_1$. The determinant is proportional to

$$\begin{aligned} d &= (x^2 + b_2^2)\omega_1^2 - 2(b_1 b_2)\omega_1\omega_2 + (b_1^2)\omega_2^2 \\ &= (\gamma^2 x^2 + \beta^2\gamma^2 b_1^2)\omega_1^2 - 2(\gamma\beta b_1^2)\gamma\omega_1^2 + (b_1^2)\gamma^2\omega_1^2 \\ &= (\gamma^2\omega_1^2)\left(x^2 + \beta^2 b_1^2 - 2(\beta b_1^2) + b_1^2\right) \\ &= (\gamma^2\omega_1^2)\left(x^2 + (\beta - 1)^2 b_1^2\right). \end{aligned}$$

This implies that necessarily $x = 0$ and $\beta = 1$. In addition, in this case, there must be a linear dependence like (47).

4) Finally, the case $a_1 \neq 0$, $b_1 = 0$ is completely analogous by exchanging the roles of a_1 and b_1. ■

To obtain the thesis in Proposition 3, we have to show that (45) is equivalent to (7). To see this, recall that $\boldsymbol{s}^k$ is obtained from $\boldsymbol{r}^k$ by conjugation ($\boldsymbol{s}^k = \ominus\boldsymbol{\ell} \oplus \boldsymbol{r}^k \oplus \boldsymbol{\ell}$), and that the matrix logarithm satisfies the property $\mathrm{Log}(\boldsymbol{A}\boldsymbol{X}\boldsymbol{A}^{-1}) = \boldsymbol{A}\,\mathrm{Log}(\boldsymbol{X})\,\boldsymbol{A}^{-1}$. It follows that $\mathrm{Log}(\boldsymbol{s}^k) = \mathrm{Log}(\boldsymbol{r}^k)$, and therefore, (45) and (7) are equivalent.

Lemma 8 (Exponential map for SE(2) [40, Lemma 1]): The exponential map Exp: $\mathrm{se}(2) \to \mathrm{SE}(2)$ can be written as

$$\mathrm{Exp}\left(t \begin{pmatrix} 0 & \omega & a \\ -\omega & 0 & b \\ 0 & 0 & 0 \end{pmatrix}\right) = \begin{pmatrix} R(\omega t) & \Psi(\omega t) \begin{pmatrix} at \\ bt \end{pmatrix} \\ 0 \qquad\qquad & 1 \end{pmatrix}$$

with

$$\Psi(\omega t) = \begin{pmatrix} \dfrac{\sin(\omega t)}{\omega t} & \dfrac{\cos(\omega t) - 1}{\omega t} \\ \dfrac{1 - \cos(\omega t)}{\omega t} & \dfrac{\sin(\omega t)}{\omega t} \end{pmatrix}.$$

APPENDIX C
OPTIMAL TRAJECTORIES FOR ESTIMATING $\hat{J}_{21}, \hat{J}_{22}$

We can characterize precisely which trajectories are optimal for the linear part of the problem.

Proposition 9: Suppose that the allowable wheels angular velocities are bounded

$$|\omega_{\mathrm{L}}|, |\omega_{\mathrm{R}}| \leq \omega_{\max}. \tag{52}$$

Consider the problem of minimizing the uncertainty of the estimates $\hat{J}_{21}, \hat{J}_{22}$, either in the mean square error and uncertainty ellipsoid size. Assume that the variation of σ_θ^k is negligible. Then, the commands profiles containing an equal number of piecewise constant tracts with values $[\pm\omega_{\max}, \mp\omega_{\max}]$ and $[\pm\omega_{\max}, \pm\omega_{\max}]$ (values are specified up to sign) obtain a value which is $\mathcal{O}(1/K)$-optimal (i.e., closer to optimal as the number of intervals K grows).

Proof: The proof is based on elementary algebraic manipulation of the closed-form covariance matrix, which is readily available because estimating $\hat{J}_{21}, \hat{J}_{22}$ is a linear problem. The covariance matrix of the estimates for these two parameters is given by $\boldsymbol{P}_J^{-1} = \sum_k \boldsymbol{L}_k^T \boldsymbol{L}_k / \left(\sigma_\theta^k\right)^2$ [as shown in (11)]. We consider optimality with respect to the mean square error [i.e., minimizing $\mathrm{Tr}(\boldsymbol{P}_J)$] as well in the entropy sense [i.e., minimizing $\det(\boldsymbol{P}_J)$].

Assume, without loss of generality, that we are considering equispaced intervals ($T^k = 1$). If σ_θ^k is constant, it can be taken to be 1. In this case, from (10), it follows that the elements of $\boldsymbol{L}_k^T = (\Delta_L^k \ \Delta_R^k)^T$ are the total angular rotations of the wheels during the kth interval. The elements of $\boldsymbol{P}_J^{-1}$ are

$$\boldsymbol{P}_J^{-1} = \begin{pmatrix} \sum (\Delta_L^k)^2 & \sum \Delta_R^k \Delta_L^k \\ \sum \Delta_R^k \Delta_L^k & \sum (\Delta_L^k)^2 \end{pmatrix}.$$

Note that the entries are the sample *second moment matrix* of the vector $(\Delta_L^k \ \Delta_R^k)^T$. This is *not* the sample covariance matrix of $(\Delta_L^k \ \Delta_R^k)^T$, unless $\sum \Delta_L^k = \sum \Delta_R^k = 0$. Fortunately, using Proposition 14, we can restrict ourselves to considering only "balanced" trajectories, for which $\sum \Delta_L^k = \sum \Delta_R^k = 0$ and be $\mathcal{O}(1/K)$ close to optimality. (This assumption is not strictly necessary, but it makes the rest of this proof elementary.) Assuming $\sum \Delta_L^k = \sum \Delta_R^k = 0$ and for large K, we can write $\boldsymbol{P}_J^{-1}$ as a covariance matrix $\begin{pmatrix} a^2 & \rho\, a\, b \\ \rho\, a\, b & b^2 \end{pmatrix}$, with $a^2 = \mathbb{E}\{(\Delta_L^k)^2\}$, $b^2 = \mathbb{E}\{(\Delta_R^k)^2\}$, and $\rho = \mathrm{corr}(\Delta_R^k, \Delta_L^k)$ is the sample correlation of the wheels velocities. The trace and the determinant of $\boldsymbol{P}_J$ can be written as

$$\mathrm{Tr}(\boldsymbol{P}_J) = \frac{1}{(1-\rho^2)} \frac{1}{a^2 b^2} \tag{53}$$

$$\det(\boldsymbol{P}_J) = \frac{1}{(1-\rho^2)} \left(\frac{1}{a^2} + \frac{1}{b^2}\right). \tag{54}$$

In either case, to minimize the uncertainty, we need to maximize a^2, b^2, and minimize ρ^2. The values of $a^2 = \mathbb{E}\{(\Delta_L^k)^2\}$ and $b^2 = \mathbb{E}\{(\Delta_R^k)^2\}$ are maximized by choosing always the extremal velocities in (52). The value of ρ^2 is minimized by choosing the trajectories such that, on average, the values of left and right wheel velocities are uncorrelated. It follows that a command profile that alternates intervals of $(\omega_{\mathrm{L}}, \omega_{\mathrm{R}}) = [+\omega_{\max}, -\omega_{\max}]$ and $(\omega_{\mathrm{L}}, \omega_{\mathrm{R}}) = [+\omega_{\max}, +\omega_{\max}]$ is a feasible solution [as it respects the constraint (52)] that is a global minimizer of both (53) and (54); hence, it is a global optimum. By Lemma 11, these trajectories are specified up to sign. ■

1) Supporting Lemmas Regarding Balanced Trajectories: This section contains some results in support of the proof of Proposition 9, that allow us to consider only "balanced" trajectories as candidates for optimality. Let Δ_L^k be the total left wheel rotation during one interval and let Δ_L, Δ_R be the total rotation in one trajectory: $\Delta_L = \sum_k \Delta_L^k, \Delta_R = \sum_k \Delta_R^k$.

Definition 10: A command profile is *balanced* if the integral of the velocity commands sums to zero: $\Delta_L = \Delta_R = 0$.

Note that this does not necessarily mean that the robot returns back to the starting position. We now show that we can limit ourselves to consider only balanced trajectories. First, we show that a command profile and its opposite give the same information matrix for the calibration parameters.

Lemma 11: The information matrix of the calibration parameters is symmetric with respect to a reversal of the command profiles. The information matrix obtained using the commands profile $(\omega_{\mathrm{L}}(t)\ \omega_{\mathrm{R}}(t))^T$ coincides with the one obtained with the commands profile $(-\omega_{\mathrm{L}}(t)\ -\omega_{\mathrm{R}}(t))^T$.

Proof: The ultimate reason is that the dynamics of a differential-drive robot is reversible, in the sense that giving the opposite command profile to the robot gives the reverse motion of the platform. Let $\boldsymbol{r}$ be the robot displacement during one interval according to a certain profile $\boldsymbol{\omega}(t)$. From (4), the sensor displacement is $\boldsymbol{s} = \ominus\boldsymbol{\ell} \oplus \boldsymbol{r} \oplus \boldsymbol{\ell}$. Let $\tilde{\boldsymbol{r}}$ be the robot displacement for the opposite commands profile $\tilde{\boldsymbol{\omega}}(t) = -\boldsymbol{\omega}(t)$. Because the dynamics are reversible, it must hold that $\tilde{\boldsymbol{r}} \oplus \boldsymbol{r} = \mathbf{0}$; hence, $\tilde{\boldsymbol{r}} = \ominus\boldsymbol{r}$. For the sensor motion, we can see that $\tilde{\boldsymbol{s}} = \ominus\boldsymbol{\ell} \oplus \tilde{\boldsymbol{r}} \oplus \boldsymbol{\ell} = \ominus\boldsymbol{\ell} \oplus (\ominus\boldsymbol{r}) \oplus \boldsymbol{\ell} = \ominus\boldsymbol{s}$. If the observations $(\tilde{\boldsymbol{s}})$ for the inverted trajectory are a function of the original observations $(\boldsymbol{s})$, then they give exactly the same information regarding the calibration parameters. ■

As a corollary of this result, one can see that exchanging the sign of the commands during one of the intervals does not change the achievable accuracy. At this point, we ask whether, by selectively changing the signs of pieces of the commands profile, we can obtain a trajectory which is balanced. The answer is given by a result of Steinitz, which states that we can rearrange the signs of a set of vectors such that the norm of their sum is bounded.

Lemma 12 (Steinitz [41, Ch. 2]): Consider a set of $m \geq 2$ vectors $\{v_i\}_{i=1}^m$ in $\mathbb{R}^n$, $n \geq 1$, such that $\|v_i\|_\infty \leq c$. Then, there exists a vector of coefficients $\{x_i\}_{i=1}^m, x_i \in \{-1, +1\}$, such that $\|\sum_{i=1}^m x_i v_i\|_\infty \leq nc$.

Note that the bound given by this lemma depends on the dimension n, but not on the number of vectors m. The case $n = 1$ is easy to see algebraically, and the case $n = 2$ can be understood geometrically. Based on Steinitz's result, we can show that, for each trajectory, we can find another which gives the same information matrix, but it is approximately balanced.

Lemma 13: For each commands profile with bounded wheel velocity ($|\omega_{\mathrm{L}}|, |\omega_{\mathrm{R}}| \leq \omega_{\max}$) composed of K intervals of equal

length T, there is a command profile with the same information matrix that is approximately balanced, in the sense that $|\Delta_L|, |\Delta_R| \leq 2T\omega_{\max}$.

Proof: Because we can invert the signs of each interval without changing the information matrix (see Lemma 11), multiplying by -1 or $+1$ each of the commands values in the intervals gives a trajectory with the same information matrix. From Lemma 12, we can choose the sign such that $|\Delta_L|, |\Delta_R| \leq 2T\omega_{\max}$; note that the bound does not depend on the number of intervals. ∎

Finally, building on the previous results, we can show that if we limit ourselves to considering only balanced trajectories, we can obtain any feasible information matrix with an error which goes to zero as the number of trajectories K grows.

Proposition 14: For any commands profile of K intervals which gives the information matrix $\boldsymbol{\mathcal{I}}$ for the parameters, there is a balanced commands profile giving an information matrix $\boldsymbol{\mathcal{I}}'$ such that $\|\boldsymbol{\mathcal{I}} - \boldsymbol{\mathcal{I}}'\| / \|\boldsymbol{\mathcal{I}}\| = \mathcal{O}(1/K)$.

Proof: By Lemma 13, there is a command profile which obtains $\boldsymbol{\mathcal{I}}$ and for which $|\Delta_L|, |\Delta_R| \leq 2T\omega_{\max}$. We can obtain a balanced command profile by modifying the commands in at most two intervals and obtain an information matrix $\boldsymbol{\mathcal{I}}'$, which is close to $\boldsymbol{\mathcal{I}}$. In particular, $\|\boldsymbol{\mathcal{I}} - \boldsymbol{\mathcal{I}}'\|$ can be bounded by a constant (the information attainable during two intervals), while $\|\boldsymbol{\mathcal{I}}\|$ is proportional to the number of observations (K). Hence, as K grows, $\|\boldsymbol{\mathcal{I}} - \boldsymbol{\mathcal{I}}'\| / \|\boldsymbol{\mathcal{I}}\| = \mathcal{O}(1/K)$. ∎

APPENDIX D
OBSERVABILITY PROPERTIES FOR CANONICAL TRAJECTORIES

Proposition 9 above gives a complete characterization of the optimality of trajectories for the parameters $\hat{J}_{21}, \hat{J}_{22}$. For the other parameters b and $\boldsymbol{\ell} = (\ell_x, \ell_y, \ell_\theta)$, we cannot give a similar complete answer, because the information matrix, albeit it can be computed numerically, is not available in a closed form that can be manipulated in a simple way. Nevertheless, we can characterize several properties for the simple motions (pure rotation and pure translation). These results cannot be reused for the study of arbitrary trajectories, yet they provide useful intuition about the role of each parameter.

Lemma 15: Motions corresponding to pure translation (forward/backward) do not give any information about ℓ_x and ℓ_y, but the sensor orientation ℓ_θ is observable.

Proof: We prove this by showing that for these particular trajectories, the observations are invariant with respect to ℓ_x and ℓ_y. The observations $\boldsymbol{s}^k \in \mathrm{SE}(2)$ are the solution at time $t = T^k$ of the differential equation $\dot{\boldsymbol{s}}(t) = \boldsymbol{s}(t)\boldsymbol{\nu}(t)$, $\boldsymbol{s}(0) = \mathbf{0}$, where $\boldsymbol{\nu}(t) \in \mathrm{se}(2)$ is the sensor velocity in the sensor frame. By setting $\omega = 0$ in (41), we obtain $\nu_\theta = 0$ and

$$\nu_x = v\,\cos(-\ell_\theta), \quad \nu_y = v\sin(-\ell_\theta). \tag{55}$$

Thus, the sensor velocity $\boldsymbol{\nu}$ does not depend on ℓ_x and ℓ_y, and, consequently, the sensor displacement $\boldsymbol{s}(t)$ does not give information about those parameters. In this case, the observations do give information about ℓ_θ. From (55), one obtains $\ell_\theta = -\mathrm{arctan2}(\nu_y/v, \nu_x/v)$. ∎

Lemma 16: Motions corresponding to pure rotation do not give any information about the wheel axis b and the sensor orientation ℓ_θ; the distance of the sensor from the robot platform center ($\|(\ell_y\ \ell_x)^T\|$) is identifiable.

Proof: Let us write (ℓ_x, ℓ_y) in polar coordinates $(\varphi_\ell, \rho_\ell)$

$$\ell_x = \rho_\ell \cos\varphi_\ell, \quad \ell_y = \rho_\ell \sin\varphi_\ell.$$

The inverse relations are clearly $\rho_\ell = \|(\ell_y\ \ell_x)^T\|$ and $\varphi_\ell = \mathrm{arctan2}(\ell_y, \ell_x)$. Setting $v = 0$ and $\omega = \nu_\theta$ in (41) and using the polar notation, we obtain

$$\begin{pmatrix} \nu_x \\ \nu_y \end{pmatrix} = \omega \boldsymbol{R}(-\ell_\theta - \varphi_\ell) \begin{pmatrix} \rho_\ell \\ 0 \end{pmatrix}.$$

By taking the modulus of both sides, we obtain $\rho_\ell = \left\|(\nu_x\ \nu_y)^T\right\| / \nu_\theta$ so that ρ_ℓ is directly observable. By taking the phase of both vectors, we obtain

$$\mathrm{arctan2}(\nu_y, \nu_x) = -\ell_\theta - \varphi_\ell \quad (\text{valid for } \rho_\ell > 0).$$

This means that, from just pure rotations, we can identify only the sum of ℓ_θ and φ_ℓ, but not either term separately. ∎

REFERENCES

[1] J. Doebbler, J. Davis, J. Junkins, and J. Valasek, "Odometry and calibration methods for multi-castor vehicles," in *Proc. Int. Conf. Robot. Autom.*, May 2008, pp. 2110–2115.

[2] H. J. Von der Hardt, R. Husson, and D. Wolf, "An automatic calibration method for a multisensor system: Application to a mobile robot localization system," in *Proc. Int. Conf. Robot. Autom.*, Leuven, Belgium, May 1998, vol. 4, pp. 3141–3146.

[3] J. Borenstein and L. Feng, "Measurement and correction of systematic odometry errors in mobile robots," *IEEE Trans. Robot. Autom.*, vol. 12, no. 6, pp. 869–880, Dec. 1996.

[4] A. Kelly, "Fast and easy systematic and stochastic odometry calibration," in *Proc. Int. Conf. Intell. Robots Syst.*, Sep./Oct. 2004, vol. 4, pp. 3188–3194.

[5] T. D. Larsen, M. Bak, N. A. Andersen, and O. Ravn, "Location estimation for an autonomously guided vehicle using an augmented Kalman filter to autocalibrate the odometry," in *Proc. 1st Int. Conf. Multisource-Multisens. Inf. Fusion*, 1998.

[6] D. Caltabiano, G. Muscato, and F. Russo, "Localization and self-calibration of a robot for volcano exploration," in *Proc. Int. Conf. Robot. Autom.*, Apr./May 2004, vol. 1, pp. 586–591.

[7] A. Martinelli, N. Tomatis, and R. Siegwart, "Simultaneous localization and odometry self calibration for mobile robot," *Auton. Robots*, vol. 22, pp. 75–85, 2006.

[8] E. Foxlin, "Generalized architecture for simultaneous localization, auto-calibration, and map-building," in *Proc. Int. Conf. Intell. Robots Syst.*, 2002, vol. 1, pp. 527–533.

[9] N. Roy and S. Thrun, "Online self-calibration for mobile robots," in *Proc. Int. Conf. Robot. Autom.*, 1999, vol. 3, pp. 2292–2297.

[10] G. Antonelli, S. Chiaverini, and G. Fusco, "A calibration method for odometry of mobile robots based on the least-squares technique: Theory and experimental validation," *IEEE Trans. Robot.*, vol. 21, no. 5, pp. 994–1004, Oct. 2005.

[11] G. Antonelli and S. Chiaverini, "Linear estimation of the physical odometric parameters for differential-drive mobile robots," *Auton. Robots*, vol. 23, no. 1, pp. 59–68, 2007.

[12] G. Antonelli and S. Chiaverini, "A deterministic filter for simultaneous localization and odometry calibration of differential-drive mobile robots," in *Proc. 3rd Eur. Conf. Mobile Robots*, 2007.

[13] R. Kuemmerle, G. Grisetti, and W. Burgard, "simultaneous calibration, localization, and mapping," in *Proc. Int. Conf. Intell. Robots Syst.*, 2011, pp. 3716–3721.

[14] Q. Zhang and R. Pless, "Extrinsic calibration of a camera and laser range finder (improves camera calibration)," in *Proc. Int. Conf. Intell. Robots Syst.*, 2004, vol. 3, pp. 2301–2306.

[15] X. Brun and F. Goulette, "Modeling and calibration of coupled fish-eye CCD camera and laser range scanner for outdoor environment

reconstruction," in *Proc. 6th Int. Conf. 3-D Digital Imaging Modeling*, 2007, pp. 320–327.
[16] H. Aliakbarpour, P. Nuez, J. Prado, K. Khoshhal, and J. Dias, "An efficient algorithm for extrinsic calibration between a 3D laser range finder and a stereo camera for surveillance," in *Proc. Int. Conf. Adv. Robot.*, Jun. 2009, pp. 1–6.
[17] A. Martinelli and D. Scaramuzza, "Automatic self-calibration of a vision system during robot motion," presented at the Int. Conf. Robot. Autom., Orlando, FL, USA, 2006.
[18] A. Martinelli and R. Siegwart, "Observability properties and optimal trajectories for on-line odometry self-calibration," in *Proc. IEEE Conf. Decis. Control*, Dec. 2006, pp. 3065–3070.
[19] F. Mirzaei and S. Roumeliotis, "A Kalman filter-based algorithm for IMU-camera calibration: Observability analysis and performance evaluation," *IEEE Trans. Robot.*, vol. 24, no. 5, pp. 1143–1156, Oct. 2008.
[20] J. Hesch, A. Mourikis, and S. Roumeliotis, "Determining the camera to robot-body transformation from planar mirror reflections," in *Proc. Int. Conf. Intell. Robots Syst.*, Sep. 2008, pp. 3865–3871.
[21] J. P. Underwood, A. Hill, T. Peynot, and S. J. Scheding, "Error modeling and calibration of exteroceptive sensors for accurate mapping applications," *J. Field Robot.*, vol. 27, pp. 2–20, Jan. 2010.
[22] J. Brookshire and S. Teller, "Automatic Calibration of Multiple Coplanar Sensors," in *Proc. Robot.: Sci. Syst.*, 2011.
[23] J. Kelly and G. S. Sukhatme, "Visual-inertial sensor fusion: Localization, mapping and sensor-to-sensor self-calibration," *Int. J. Robot. Res.*, vol. 30, pp. 56–79, 2011.
[24] A. Censi, L. Marchionni, and G. Oriolo, "Simultaneous maximum-likelihood calibration of robot and sensor parameters," in *Proc. Int. Conf. Robot. Autom.*, May 2008, pp. 2098–2103.
[25] A. Martinelli, "Local decomposition and observability properties for automatic calibration in mobile robotics," in *Proc. Int. Conf. Robot. Autom.*, May 2009, pp. 4182–4188.
[26] A. Martinelli, "State estimation based on the concept of continuous symmetry and observability analysis: The case of calibration," *IEEE Trans. Robot.*, vol. 27, no. 2, pp. 239–255, Apr. 2011.
[27] G. Antonelli, F. Caccavale, F. Grossi, and A. Marino, "A non-iterative and effective procedure for simultaneous odometry and camera calibration for a differential drive mobile robot based on the singular value decomposition," *Intell. Serv. Robot.*, vol. 3, no. 3, pp. 163–173, 2010.
[28] G. Antonelli, F. Caccavale, F. Grossi, and A. Marino, "Simultaneous calibration of odometry and camera for a differential drive mobile robot," in *Proc. Int. Conf. Robot. Autom.*, 2010, pp. 5417–5422.
[29] R. M. Murray, Z. Li, and S. S. Sastry, *A Mathematical Introduction to Robotic Manipulation*, 1st ed. Boca Raton, FL, USA: CRC Press, Mar. 1994.
[30] R. Hermann and A. Krener, "Nonlinear controllability and observability," *IEEE Trans. Autom. Control*, vol. AC-22, no. 5, pp. 728–740, Oct. 1977.
[31] H. L. V. Trees and K. L. Bell, *Bayesian Bounds for Parameter Estimation and Nonlinear Filtering/Tracking*. New York, NY, USA: Wiley-IEEE Press, 2007.
[32] S. Boyd and L. Vandenberghe, *Convex Optimization*. New York, NY, USA: Cambridge Univ. Press, 2004.
[33] P. J. Rousseeuw and A. M. Leroy, *Robust Regression and Outlier Detection*, 3rd ed. New York, NY, USA: Wiley, 1996.
[34] B. Siciliano, L. Villani, L. Sciavicco, and G. Oriolo, *Robotics: Modelling, Planning and Control*. New York, NY, USA: Springer-Verlag, 2008.
[35] H. Kawata, A. Ohya, S. Yuta, W. Santosh, and T. Mori, "Development of ultra-small lightweight optical range sensor system," in *Proc. Int. Conf. Intell. Robots Syst.*, Aug. 2005, pp. 1078–1083.
[36] L. Kneip, F. T. G. Caprari, and R. Siegwart, "Characterization of the compact Hokuyo URG-04LX 2D laser range scanner," presented at the Int. Conf. Robot. Autom., Kobe, Japan, 2009.
[37] A. Censi, "An ICP variant using a point-to-line metric," in *Proc. Int. Conf. Robot. Autom.*, May 2008, pp. 19–25. [Online]. Source code Available: http://andreacensi.github.com/csm/ (Also Available as a ROS package at:http://www.ros.org/wiki/laser_scan_matcher)
[38] A. Censi, "An accurate closed-form estimate of ICP's covariance," in *Proc. Int. Conf. Robot. Autom.*, Apr. 2007, pp. 3167–3172.
[39] A. Censi, "On achievable accuracy for pose tracking," in *Proc. Int. Conf. Robot. Autom.*, Kobe, Japan, May 2009, pp. 1–7.
[40] F. Bullo and R. M. Murray, "Proportional derivative (PD) control on the Euclidean group," California Inst. Technol., Pasadena, CA, USA, Tech. Rep. Caltech/CDS 95-010, May 1995.
[41] M. Kadeŧs and V. Kadeŧs, *Series in Banach Spaces: Conditional and Unconditional Convergence* (Operator theory: Advances and applications 94). Cambridge, MA, USA: Birkhäuser-Verlag, 1997.

Andrea Censi (S'04–M'12) received the Laurea and Laurea Specialistica degrees (*summa cum laude*) in control engineering and robotics from the Sapienza University of Rome, Rome, Italy, in 2005 and 2007, respectively, and the Ph.D. degree in control and dynamical systems from the California Institute of Technology, Pasadena, CA, USA, in 2012.

He is currently a Postdoctoral Researcher with the California Institute of Technology. His research interests include perception, estimation, and learning in natural and artificial systems.

Antonio Franchi (S'07–M'11) received the Laurea degree (*summa cum laude*) in electronic engineering and the Ph.D. degree in control and system theory from the Sapienza University of Rome, Rome, Italy, in 2005 and 2009, respectively.

He was a Visiting Student with the University of California, Santa Barbara, CA, USA, in 2009. In 2010, he joined the Max Planck Institute for Biological Cybernetics, Tübingen, Germany, where he is currently a Senior Research Scientist, Head of the Human–Robot Interaction Group. His main research interests include autonomous systems and robotics, with a special regard to control, planning, estimation, human–machine interaction, haptics, and hardware/software architectures.

Luca Marchionni (S'07) received the Laurea and Laura Specialistica degrees (*summa cum laude*) in control engineering and robotics from the Sapienza University of Rome, Rome, Italy, in 2005 and 2007, respectively.

Since 2009, he has been with Pal Robotics, Barcelona, Spain, developing humanoid service robots. His interests are in the area of simultaneous localization and mapping, planning and control of robotic systems, and biped walking.

Giuseppe Oriolo (S'89–M'92–SM'02) received the Ph.D. degree in control systems engineering from Sapienza University of Rome, Rome, Italy, in 1992, where he currently teaches automatic control and robotics and heads the Robotics Laboratory.

His research interests are in the area of planning and control of robotic systems, in which he has published two books and more than 140 papers.

Dr. Oriolo is the Editor of the IEEE TRANSACTIONS ON ROBOTICS.